nature cell biology

ARTICLES

https://doi.org/10.1038/s41556-018-0260-7

An IRAK1–PIN1 signalling axis drives intrinsic tumour resistance to radiation therapy

Peter H. Liu[1,2], Richa B. Shah[1,2], Yuanyuan Li[1,2], Arshi Arora[3], Peter Man-Un Ung[4], Renuka Raman[1,2], Andrej Gorbatenko[5], Shingo Kozono[6], Xiao Zhen Zhou[6], Vincent Brechin[1,2,10], John M. Barbaro[1,2,11], Ruth Thompson[1,2,12], Richard M. White[7], Julio A. Aguirre-Ghiso[1], John V. Heymach[8], Kun Ping Lu[6], Jose M. Silva[5], Katherine S. Panageas[3], Avner Schlessinger[4], Robert G. Maki[1,2,13], Heath D. Skinner[8], Elisa de Stanchina[9] and Samuel Sidi[1,2*]

Drug-based strategies to overcome tumour resistance to radiotherapy (R-RT) remain limited by the single-agent toxicity of traditional radiosensitizers (for example, platinums) and a lack of targeted alternatives. In a screen for compounds that restore radiosensitivity in *p53* mutant zebrafish while tolerated in non-irradiated wild-type animals, we identified the benzimidazole anthelmintic oxfendazole. Surprisingly, oxfendazole acts via the inhibition of IRAK1, a kinase thus far implicated in interleukin-1 receptor (IL-1R) and Toll-like receptor (TLR) immune responses. IRAK1 drives R-RT in a pathway involving IRAK4 and TRAF6 but not the IL-1R/TLR–IRAK adaptor MyD88. Rather than stimulating nuclear factor-κB, radiation-activated IRAK1 prevented apoptosis mediated by the PIDDosome complex (comprising PIDD, RAIDD and caspase-2). Countering this pathway with IRAK1 inhibitors suppressed R-RT in tumour models derived from cancers in which *TP53* mutations predict R-RT. Moreover, IRAK1 inhibitors synergized with inhibitors of PIN1 a prolyl isomerase essential for IRAK1 activation, in response to pathogens and as shown here, ionizing radiation. These data identify an IRAK1 radiation-response pathway as a rational chemoradiation therapy target.

Radiotherapy induces cytotoxic DNA breaks in tumour cells while minimizing damage to healthy tissues, and is given to ~60% of patients with cancer over the course of treatment[1,2]. Current approaches to overcoming tumour R-RT consist of concurrent systemic chemotherapy with classical anticancer agents such as genotoxins (for example, cisplatin and 5-fluorouracil) and microtubule inhibitors (for example, taxanes). These traditional radiosensitizers primarily act by augmenting DNA damage levels, thus enhancing cell killing within the field of radiation[1–4]. Radiosensitizers can be effective; for example, cisplatin-based chemoradiation therapy (CRT) improves survival by 10% compared to RT alone in patients with head and neck squamous cell carcinoma (HNSCC) and is the current standard of care in this cancer[5]. However, tumours recur in a large majority of patients, leading to invariably fatal disease. Further improvements of CRT have remained limited by the toxicity of radiosensitizers as single agents[2,3]. Moreover, these genotoxic drugs were not designed against—and thus do not necessarily target—the genetic defects or signalling pathways that drive tumour R-RT. Devising targeted strategies to supplant these cytotoxic chemotherapies is a current central focus of the Radiation Therapy Oncology Group of the US National Cancer Institute[1] and the Clinical and Translational Radiotherapy Research Working Group of the The National Cancer Research Institute (UK)[2].

A candidate and potentially pervasive mechanism of tumour R-RT is mutation of the p53 transcription factor, which occurs in ~50% of solid tumours[6]. Cells with mutant p53 fail to initiate apoptotic or senescence gene-expression programmes in response to ionizing radiation (IR)-induced DNA breaks[7–9]. In HNSCC[10,11], colorectal cancer (CRC)[12,13], breast cancer[14], glioblastoma[15] and medulloblastoma[16], patients with missense *TP53* mutations have markedly worse outcomes following RT or CRT compared with patients with wild-type (WT) *TP53*, with declines in recurrence-free or overall survival ranging from ~33% to 100%. Yet, patients are not stratified by *TP53* status and there are currently no drugs reported to improve RT outcomes in *TP53* mutant tumours[1,2].

Results

In vivo zebrafish radiosensitizer screen identifies oxfendazole. To identify such genotype-directed radiosensitizers while accounting for the problem of systemic toxicity, we developed a whole-animal model of mutant *TP53*-driven R-RT for use in unbiased genetic and chemical screens[17,18]. In this model, zebrafish embryos

[1]Department of Medicine, Division of Hematology and Medical Oncology, Tisch Cancer Institute, Icahn School of Medicine at Mount Sinai, New York, NY, USA. [2]Department of Cell, Developmental and Regenerative Biology, The Graduate School of Biomedical Sciences, Icahn School of Medicine at Mount Sinai, New York, NY, USA. [3]Department of Epidemiology and Biostatistics, Memorial Sloan Kettering Cancer Center, New York, NY, USA. [4]Department of Pharmacological Sciences, Icahn School of Medicine at Mount Sinai, New York, NY, USA. [5]Department of Pathology, Tisch Cancer Institute, Icahn School of Medicine at Mount Sinai, New York, NY, USA. [6]Cancer Biology Program, Beth Israel Deaconess Medical Center, Harvard Medical School, Boston, MA, USA. [7]Department of Cancer Biology and Genetics, Memorial Sloan Kettering Cancer Center, New York, NY, USA. [8]Department of Thoracic/Head and Neck Medical Oncology, The University of Texas MD Anderson Cancer Center, Houston, TX, USA. [9]Antitumor Assessment Core and Molecular Pharmacology Department, Memorial Sloan Kettering Cancer Center, New York, NY, USA. [10]Present address: Institute of Molecular and Cellular Biosciences, The University of Tokyo, Tokyo, Japan. [11]Present address: Albert Einstein College of Medicine, Bronx, NY, USA. [12]Present address: Department of Oncology and Metabolism, The University of Sheffield, Sheffield, UK. [13]Present address: Hofstra-Northwell School of Medicine and Cold Spring Harbor Laboratory, Hempstead, NY, USA. *e-mail: samuel.sidi@mssm.edu

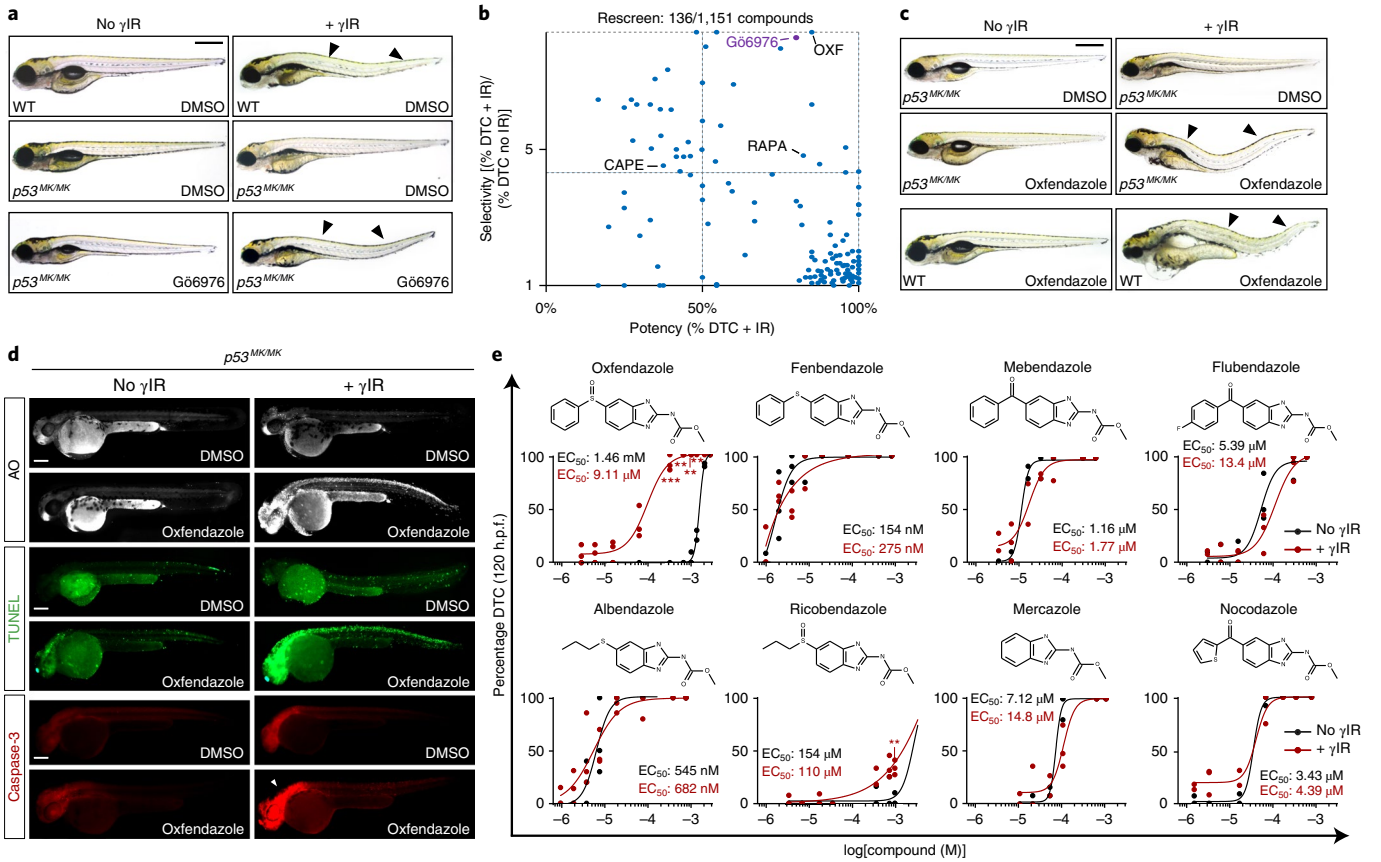

Fig. 1 | In vivo zebrafish drug screen identifies oxfendazole as a radiosensitizer of *p53* mutant embryos. a, ^{37}Cs-irradiated *p53*$^{MK/MK}$ zebrafish embryos (15 Gy total body irradiation (TBI) at 18 h.p.f.) observed at 120 h.p.f. lack the DTC phenotype of WT embryos (arrowheads indicate a late readout of embryonic radiosensitivity). DTCs are restored with a CHK1 inhibitor (Gö6976, 1 μM) in an average of 75% of mutants per experiment (Supplementary Fig. 1d). **b**, Rescreen of the top 136 hits from a primary screen (Supplementary Fig. 1c–g) scored for potency (percentage of DTC after γIR) and selectivity ((percentage of DTC after γIR)/(percentage of DTC without γIR)), identifying oxfendazole (OXF) as the top hit. Capecitabine (CAPE) and rapamycin (RAPA), two known clinical radiosensitizers, were also recovered in the blind screen, providing internal validation of the DTC assay. **c**, Doses of oxfendazole (shown here, 63 μM) that suppress R-RT in *p53*$^{MK/MK}$ embryos are fully tolerated in the absence of γIR, including in WT animals. **d**, *p53*$^{MK/MK}$ mutants treated with oxfendazole + IR score positive for acridine orange (AO), a vital marker of cell death, and apoptosis markers (TUNEL and anti-active caspase-3) at 48 h.p.f. **e**, Structure–activity relationship of benzimidazole tubulin-binding analogues in dose–response curves for 120 h.p.f. *p53*$^{MK/MK}$ embryos scored for DTCs. The chemical structure of each analogue is shown. Black curves, no IR. Red curves, 15 Gy TBI delivered at 18 h.p.f. Data are shown as the mean of $n = 3$ independent experiments for oxfendazole without IR (10–40 μM), oxfendazole + IR (0.1–40 μM), flubendazole without IR (0.1–10 μM), flubendazole + IR (0.1–10 μM), albendazole without IR (0.05–0.2 μM), albendazole + IR (0.05–2.0 μM), mebendazole without IR (0.2–2.0 μM), mebendazole + IR (0.1–2.0 μM), fenbendazole without IR (0.05–0.1 μM), fenbendazole + IR (0.025–0.1 μM), ricobendazole without IR (20–75 μM), ricobendazole + IR (20–75 μM), mercazole without IR (2 μM), mercazole + IR (2 μM). $n = 2$ independent experiments for the remaining data points, as indicated by the dot plots and as detailed in Supplementary Fig. 5, with >21 embryos scored per experiment. $^{**}P < 0.005$, $^{***}P < 0.0005$ (two-tailed Student's t-test, $\alpha = 0.05$). See Supplementary Table 4 for statistics source data, including precise *P* values. Scale bars, 0.5 mm (**a**,**c**) and 0.2 mm (**d**).

homozygous for the M214K (MK) mutation in *tp53* display fully penetrant R-RT. This is evidenced by a complete lack of cell death induction in response to IR, a phenotype scored in 24–48 h post fertilization (h.p.f.) embryos[17,18] (Supplementary Fig. 1a,b). Moreover, *p53*$^{MK/MK}$ mutants exhibit a complete lack of IR-induced dorsal tail curvatures (DTCs), a morphological manifestation of zebrafish radiosensitivity[19] assessable by eye in 96–120 h.p.f. larvae (Fig. 1a). The mutated M214 residue corresponds to M246 in human p53, which maps to the mutational hotspot region in the DNA-binding domain and is mutated in >150 human tumours sequenced thus far[6]. In a pilot candidate gene-based screen, we found that inhibitors of checkpoint kinase 1 (CHK1), such as Gö6976, restore WT levels of IR-induced cell death in *p53*$^{MK/MK}$ embryos, with minimal toxicity in the absence of IR[18] (Supplementary Fig. 1a,b). Such potent radiosensitization by means of CHK1 inhibition was also evident in the late DTC assay, whereby Gö6976 restored DTC formation in ~75% of the mutants with no effects in the absence of IR (Fig. 1a,b; Supplementary Fig. 1d). Gö6976 therefore provided a positive control for large-scale radiosensitizer screens exploiting the morphological DTC phenotype as a readout.

In a screen of 1,151 small molecules (including 640 drugs approved by the US Food and Drug Administration (FDA)), we identified one compound, oxfendazole, which radiosensitized *p53*$^{MK/MK}$ mutants with both greater potency and lesser toxicity than Gö6976 (Fig. 1b; Supplementary Fig. 1c–g; Supplementary Tables 1 and 2). Importantly, these effects were observed at concentrations tolerated by non-irradiated WT embryos (Fig. 1c). Radiosensitization by oxfendazole was retained in mutant p53-depleted *p53*$^{MK/MK}$ embryos (Supplementary Fig. 2a–c) and was apoptotic in nature, as evidenced by acridine orange, TUNEL

(TdT-mediated dUTP nick end labelling) and active caspase-3 stains of 48 h.p.f. embryos examined 30 h post-IR (hpIR) (Fig. 1d). Oxfendazole-mediated radiosensitization was also associated with an increase in DNA damage levels (Supplementary Fig. 2d,e), and was dose- and time-dependent, with maximal efficacy when administered 0–4 hpIR (Supplementary Fig. 2g–i).

Target discovery for oxfendazole identifies IRAK1. Oxfendazole is a benzimidazole anthelmintic approved for the treatment of worm infections in livestock[20,21]. Because other microtubule inhibitors, such as taxanes, are commonly used as radiosensitizers[4], we initially considered tubulin inhibition as the mechanism for oxfendazole-mediated radiosensitization. Unexpectedly, none of seven tubulin-binding analogues of oxfendazole, including the classical antimitotic nocodazole, could phenocopy the drug (the in vivo structure–activity relationship is shown in Fig. 1e). Specifically, while the analogues could produce DTCs as efficiently as oxfendazole, none showed any selectivity for IR (with the possible exception of ricobendazole) and induced DTCs in the mutants regardless of radiation (Fig. 1e). Thus, tubulin inhibition is unlikely to fully account for, if even involved in, the radiosensitizing properties of oxfendazole. It is notable in this regard that of all the benzimidazoles tested, oxfendazole and ricobendazole have the lowest affinity for tubulin[20].

To identify the novel target (or targets) of oxfendazole whose inhibition might drive radiosensitization, we used the similarity ensemble approach (SEA) target-prediction algorithm[22] (Fig. 2a). SEA yielded 12 candidate targets, which we then tested for their ability to phenocopy oxfendazole when inhibited by specific inhibitors in vivo (Fig. 2b; Supplementary Fig. 2j). This analysis identified the IL-1 receptor (IL-1R)-associated kinases IRAK1 and IRAK4[23,24] as targets, and inhibition of these by an IRAK1/4 kinase inhibitor[25] radiosensitized *p53*$^{MK/MK}$ embryos with a potency nearing that of oxfendazole (Figs. 2b–d and 3a; Supplementary Fig. 2j). Kinase-binding and in vitro kinase assays demonstrated that oxfendazole is a selective IRAK1 inhibitor (Fig. 2h,i). The observed dissociation constant (K_d of 5.8 μM) and half-maximum inhibitory concentration (IC_{50} of 38 μM) were consistent with concentrations of oxfendazole that radiosensitize zebrafish *p53*$^{MK/MK}$ mutants (Fig. 1e). Docking of oxfendazole onto IRAK4-derived zebrafish and human IRAK1 models[26] predicted drug binding to the ATP-binding site and an interaction with the hinge region via the benzimidazolyl carbamate moiety, while the phenylsulfoxide moiety resides in a pocket adjacent to the DFG motif (Fig. 2e–g).

IRAK1 is known as an effector of the IL-1R and TLRs in innate immune signalling[27]. It acts through the TRAF6 E3 ubiquitin ligase to stimulate nuclear factor-κB (NF-κB), p38 MAPK, JNK and ERK prosurvival and inflammatory responses to pathogens[23,24]. IRAK1 had not been previously implicated in the DNA damage response or cellular response to RT. Yet, inspection of The Cancer Genome Atlas (TCGA) cohort revealed significant overexpression of *IRAK1* in HNSCC and breast cancer samples harbouring *TP53* mutant genotypes compared to WT, as well as tumours from patients with breast cancer who ultimately received RT as part of their treatment (Supplementary Fig. 3a,i,j; $P < 0.0001$, $P < 0.0001$ and $P < 0.05$, respectively, Wilcoxon rank-sum test). We also found that IRAK1 is commonly activated in response to IR in *TP53* mutant HNSCC-, breast cancer- and CRC-derived cell lines, correlating with pronounced R-RT phenotypes (Fig. 5d,g,h). We therefore further investigated IRAK1 as a target for inhibition in tumour R-RT.

We first sought to confirm the oxfendazole and IRAK1/4 inhibitor data with additional IRAK1 inhibitors and gene targeting in zebrafish *p53*$^{MK/MK}$ embryos, as well as *TP53* mutant human cancer cells. For IRAK1 inhibition, we selected the tyrosine kinase inhibitor R406, which inhibits IRAK1 with an IC_{50} of 9.7 nM compared with 150 nM for IRAK4[28], and ginsenoside-Rb1, a ginseng extract that inhibits IRAK1 but not IRAK4 or IRAK2[29]. Whether in zebrafish *p53*$^{MK/MK}$ mutants, HeLa cells (devoid of p53 protein via human papillomavirus E6) or *TP53* mutant or null human cancer cell lines, genetic or pharmacological inhibition of IRAK1 was consistently incompatible with cell survival in the presence of IR but tolerated in the absence of IR (Figs. 2j, 3a–f, 4a and 5e; Supplementary Fig. 4a–f). Both the zebrafish and human cell *IRAK1* knockdown models were rescued by WT but not kinase dead[30] (KD) human IRAK1 (Figs. 3e–g and 4c). Importantly, overexpression of WT, but not KD, IRAK1 was sufficient to confer R-RT to otherwise radiosensitive Daoy MB cells (Fig. 4b). Finally, CRISPR (clustered regularly interspaced short palindromic repeats)–Cas9 gene editing confirmed the essential requirement of the kinase for cell survival specifically after IR (Fig. 4d).

IRAK1 drives R-RT independently of its IL-1R/TLR adaptor MyD88 and of canonical downstream pathways. Both the proximal activator and proximal effector of IRAK1 in IL-1R and TLR signalling—IRAK4 and TRAF6, respectively[23,24,27]—were also required for cell survival after IR (Fig. 4e). IRAK4 was necessary for IR-induced activation of IRAK1, as assessed by T209 phosphorylation[31,32] (Fig. 4f), while an IRAK1 mutant deficient in TRAF6-binding, IRAK1^{E3A} (E544A/E587A/E706A)[33], afforded only partial rescue of *irak1*-depleted *p53*$^{MK/MK}$ embryos (Fig. 3e–g). By contrast, the adaptor protein MyD88—which bridges IRAK1 and IRAK4 to IL-1R and TLRs and is essential for IRAK1 and IRAK4 activation in innate immunity[23,24,27,34]—was dispensable for both IR-induced IRAK1 T209 phosphorylation and overall R-RT in HeLa cells and *p53*$^{MK/MK}$ zebrafish (Fig. 4e–i; Supplementary Fig. 4g,k,l). In further contrast to canonical IRAK1 immune signalling, the kinase did not engage NF-κB, p38 MAPK, JNK or ERK signalling in response to IR (Fig. 4j; Supplementary Fig. 4h). Moreover, an IRAK1 mutant deficient in NF-κB essential modulator (NEMO) binding, IRAK1^{K2R} (K134R/K180R)[35], restored R-RT in IRAK1-depleted *p53*$^{MK/MK}$ zebrafish as efficiently as WT IRAK1 (Fig. 3e–g).

IR-activated IRAK1 acts to suppress PIDDosome-mediated apoptosis. Instead of acting through its aforementioned canonical signalling pathways, we found that IRAK1 drives survival after IR by preventing PIDDosome (PIDD–RAIDD–caspase-2) signalling, a DNA damage-inducible apoptotic axis that does not require p53 for activation or function after IR[36–38]. Indeed, depletion or deletion of IRAK1 triggered caspase-2 maturation in irradiated cells in a *PIDD*- and *RAIDD*-dependent manner (Fig. 4k,l; Supplementary Fig. 4i,j). Moreover, IRAK1 inhibitor-mediated radiosensitization was abolished in cells depleted of PIDD, RAIDD or caspase-2[36] (Fig. 4m,n). As expected from previous studies[36,39], PIDDosome-mediated radiosensitization was associated with increased levels of DNA damage (Supplementary Fig. 2f). Finally, IRAK1 inhibition after IR was sufficient to enable ATM-mediated phosphorylation of the PIDD death domain (PIDDpT788) (Fig. 4k; Supplementary Fig. 4i), an event necessary and sufficient for RAIDD recruitment and PIDDosome formation[36]. Together, these data point to an evolutionarily conserved role for IRAK1 in protecting cells against IR-induced cell death, acting in a pathway related to, but genetically distinct from, IL-1R/TLR signalling.

IRAK1 inhibitors restore radiosensitivity in multiple cell models of tumour R-RT. To evaluate the robustness of the IRAK1-targeting strategy, we analysed the radiosensitizing properties of IRAK1 inhibitors across both tumour and *TP53* mutation spectra. We assembled a panel of relevant cancer cell lines based on the following three criteria: they must originate from a tumour type in which *TP53* mutations adversely affect patient survival after RT or CRT; they must contain a non-synonymous mutation in *TP53*; and they must have been previously demonstrated as radioresistant in clonogenic assays. A search of the Cancer Cell Line Encyclopedia[40]

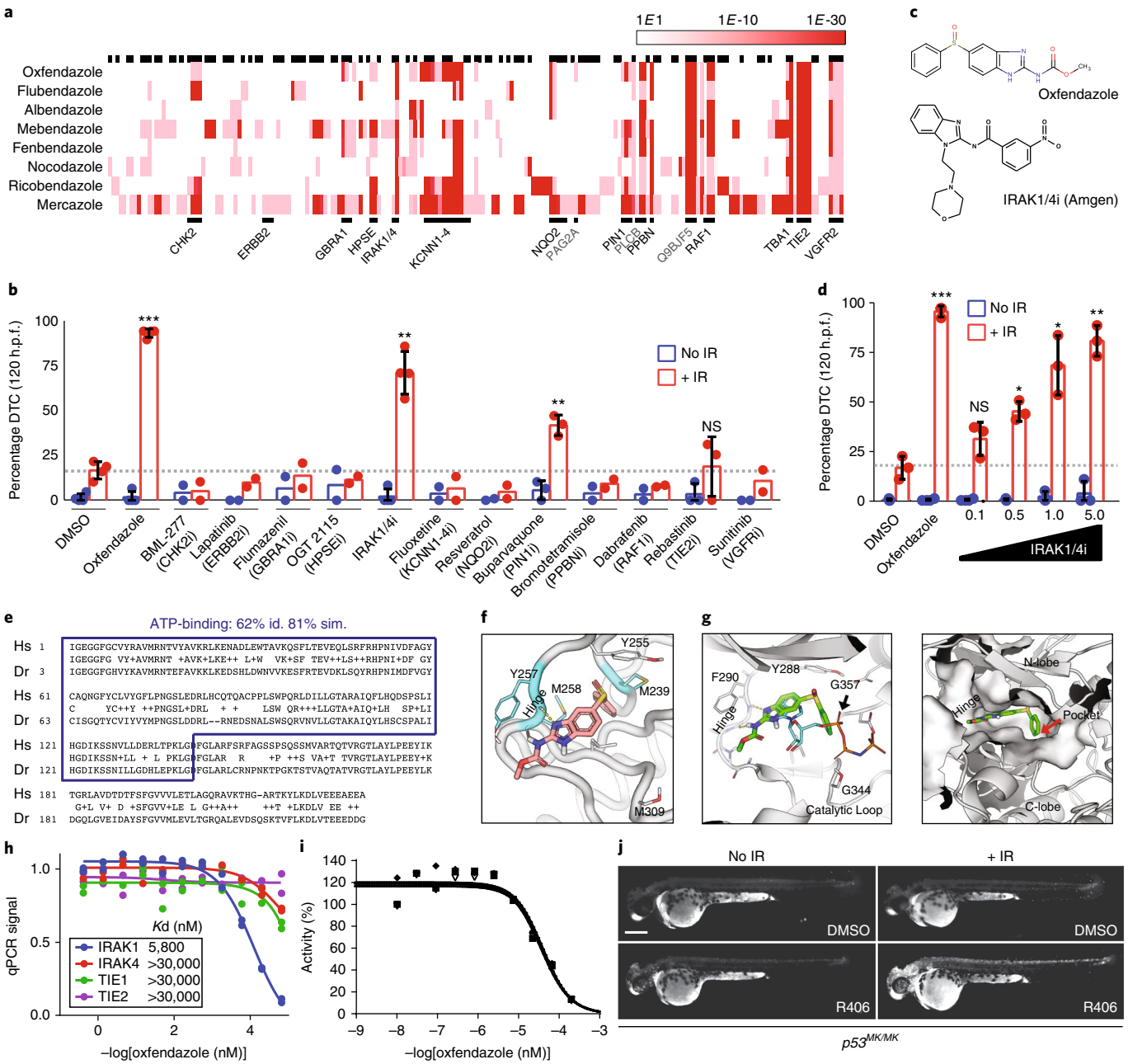

Fig. 2 | Target discovery for oxfendazole identifies IRAK1. a, SEA-predicted targets of oxfendazole and analogues. The *E*-value is colour-coded white to red. Black bars represent predicted targets for oxfendazole. **b**, DTC assay of $p53^{MK/MK}$ embryos (120 h.p.f.) treated with inhibitors of SEA-predicted oxfendazole targets (**a**) with or without 15 Gy γIR. The dotted line represents the penetrance cut-off at DMSO + IR levels. Data are presented as the mean ± s.d. of $n = 4$ independent experiments (DMSO, IRAK1/4 inhibitor (IRAK1/4i)), $n = 3$ independent experiments (oxfendazole, buparvaquone, rebastinib) or $n = 2$ independent experiments (remaining drugs) with >12 embryos per experiment. $^{**}P < 0.005$, $^{***}P < 0.0005$ relative to DMSO-treated irradiated embryos (bar 2; two-tailed Student's *t*-test). **c**, Chemical structures of indicated drugs. **d**, Dose–response to IRAK1/4 inhibitor (μg ml^{-1}) of $p53^{MK/MK}$ embryos scored in DTC assays. Data are presented as the mean ± s.d. of $n = 3$ independent experiments. $^{*}P < 0.05$, $^{**}P < 0.005$, $^{***}P < 0.0005$ relative to DMSO-treated irradiated embryos (bar 2; two-tailed Student's *t*-test). **e**, Sequence alignment of human (Hs) and zebrafish (Dr) IRAK1 kinase domains, ATP-binding domain boxed in blue. Id, identity, sim., similarity. **f**,**g**, Induced-fit docking of oxfendazole to ATP-binding site of zebrafish (**f**) and human (**g**) IRAK1 models. Gate-keeper residue, Y255 (Y288 in human). Three residue changes near the proposed docking pose within the binding site is highlighted in cyan in the zebrafish model: M239, Y257 and M258 (V272, F290 and L291 in the human model). **h**,**i**, KINOMEScan in vitro kinase capture assay for indicated kinases (**h**) and in vitro kinase assay versus IRAK1 (**i**), curved-fit from two and three replicates, respectively. **j**, The IRAK1 inhibitor R406 (40 μg ml^{-1}) phenocopies oxfendazole (Fig. 1d) in an AO assay at 48 h.p.f., with images representative of two independent experiments. See Supplementary Table 4 for statistics source data, including precise *P* values. Scale bar, 0.2 mm.

combined with a literature search identified 12 such lines derived from HNSCC, medulloblastoma, glioblastoma, CRC and breast cancer (Fig. 5d). We also included MCF7 cells, which, while WT for *TP53*, display profound resistance to IR due to deletion of *CASP3*[41]. With the exception of the Daoy MB line, all selected cell lines were confirmed as radioresistant in response to 2.5, 5 and up to 7.5 Gy

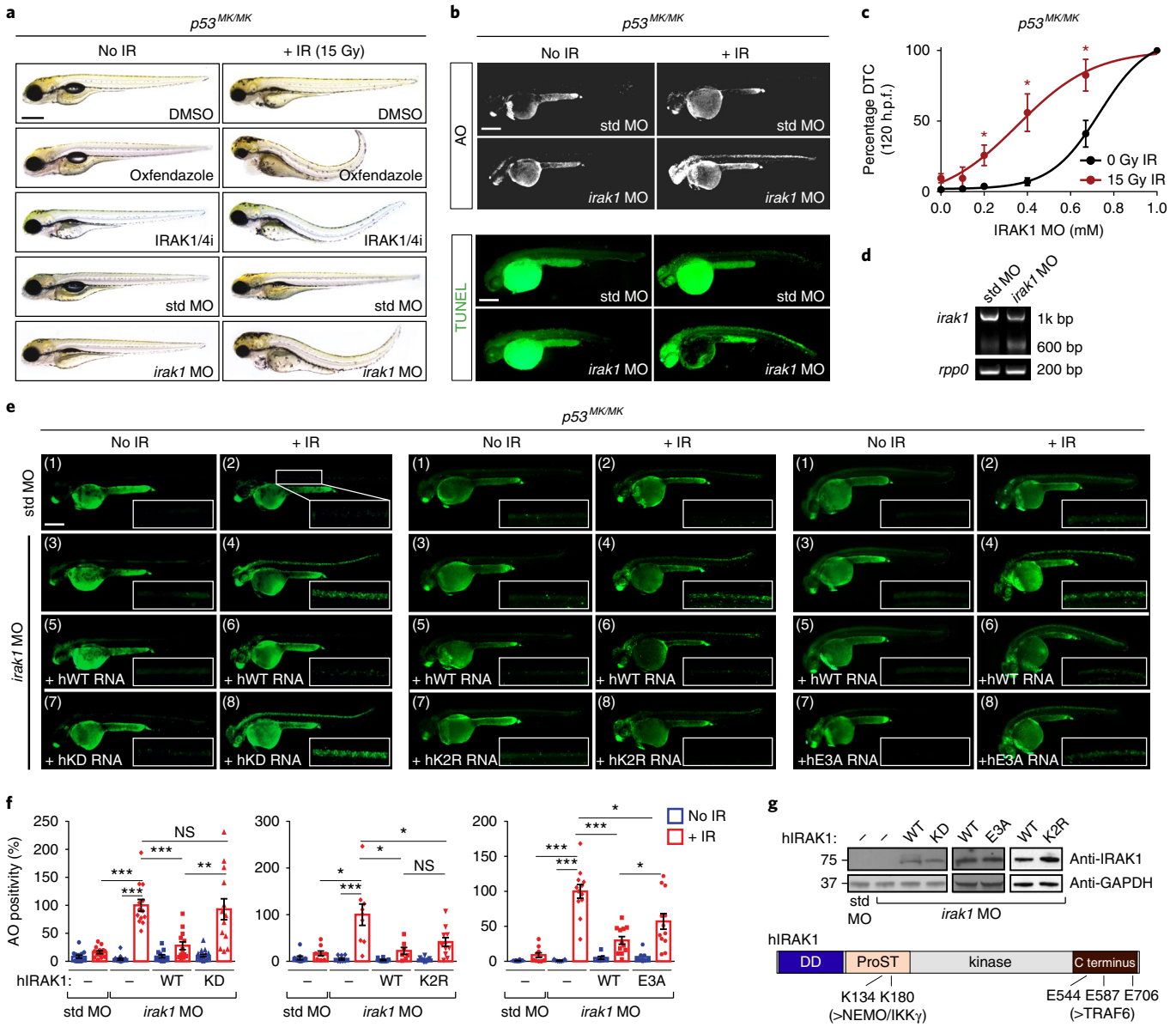

Fig. 3 | Targeting *irak1* overcomes R-RT in *p53*$^{MK/MK}$ zebrafish. a–c, Morpholino (MO) depletion of *irak1* phenocopies oxfendazole and IRAK1/4 inhibitor (IRAK1/4i) in DTC (**a**), AO (**b**, top) and TUNEL (**b**, bottom) assays (oxfendazole shown in Fig. 1d). MO dose-response in *p53*$^{MK/MK}$ embryos in the DTC assay (**c**). Data are the mean ± s.d. of $n = 3$ independent experiments. **d**, RT-PCR of pooled embryonic extracts showing reduced WT mRNA levels (upper band) and skipping of exon 4 (lower band). *rpp0*, ribosomal protein P0. **e**,**f**, Representative images (**e**) and quantification (**f**) of *irak1*-depleted *p53*$^{MK/MK}$ embryos reconstituted with WT versus KD (left), WT versus IRAK1^{K2R} (K2R, middle) or WT versus IRAK1^{E3A} (E3A, right) human IRAK1 (hIRAK1) mRNA scored in AO assays. Number of quantified, independent images (as boxed in **e**) for each column of images is as follows. Left: std MO + mock: n of non-irradiated = 14, n of irradiated = 14; *irak1* MO + mock: n of non-irradiated = 13, n of irradiated = 13; *irak1* MO + WT: n of non-irradiated = 12, n of irradiated = 13; *irak1* MO + KD: n of non-irradiated = 15, n of irradiated = 13. Middle: std MO + mock: n of non-irradiated = 9, n of irradiated = 9; *irak1* MO + mock: n of non-irradiated = 9, n of irradiated = 9; *irak1* MO + WT: n of non-irradiated = 8, n of irradiated = 7; *irak1* MO + KD: n of non-irradiated = 10, n of irradiated = 11. Right: std MO + mock: n of non-irradiated = 8, n of irradiated = 10; *irak1* MO + mock: n of non-irradiated = 7, n of irradiated = 12; *irak1* MO + WT: n of non-irradiated = 7, n of irradiated = 12; *irak1* MO + KD: n of non-irradiated = 8, n of irradiated = 12. Raw images of all embryos and cropped spinal chord areas are available at https://doi.org/10.6084/m9.figshare.7427942. **g**, Western blot of embryonic extracts showing hIRAK1 levels and diagram of hIRAK1, with disrupted residues and interactions shown. All data are presented as the mean ± s.d., $^*P < 0.05$, $^{**}P < 0.005$, $^{***}P < 0.0005$ (two-tailed Student's *t*-test). See Supplementary Table 4 for statistics source data, including precise *P* values, and Supplementary Fig. 8 for unprocessed immunoblots. Scale bars, 0.5 mm (**a**) and 0.2 mm (**b**,**e**).

IR (see Fig. 5b–d and Supplementary Fig. 5 for dimethylsulfoxide (DMSO) columns and corresponding cell viability curves). We therefore screened the panel with the IRAK1 inhibitors R406 and ginsenoside-Rb1 applied at their respective maximum tolerated doses (MTDs), as determined in HeLa cells (Fig. 5a), as well as a twofold higher dose (2×MTD). For comparison, we tested cisplatin (MTD and 2×MTD, as above), whose combination with RT is a standard of care in HNSCC and is commonly used in CRT of many other cancers[2]. Cisplatin failed to sensitize any of the *TP53* mutant lines to IR, with only marginal additive effects observed in YD38

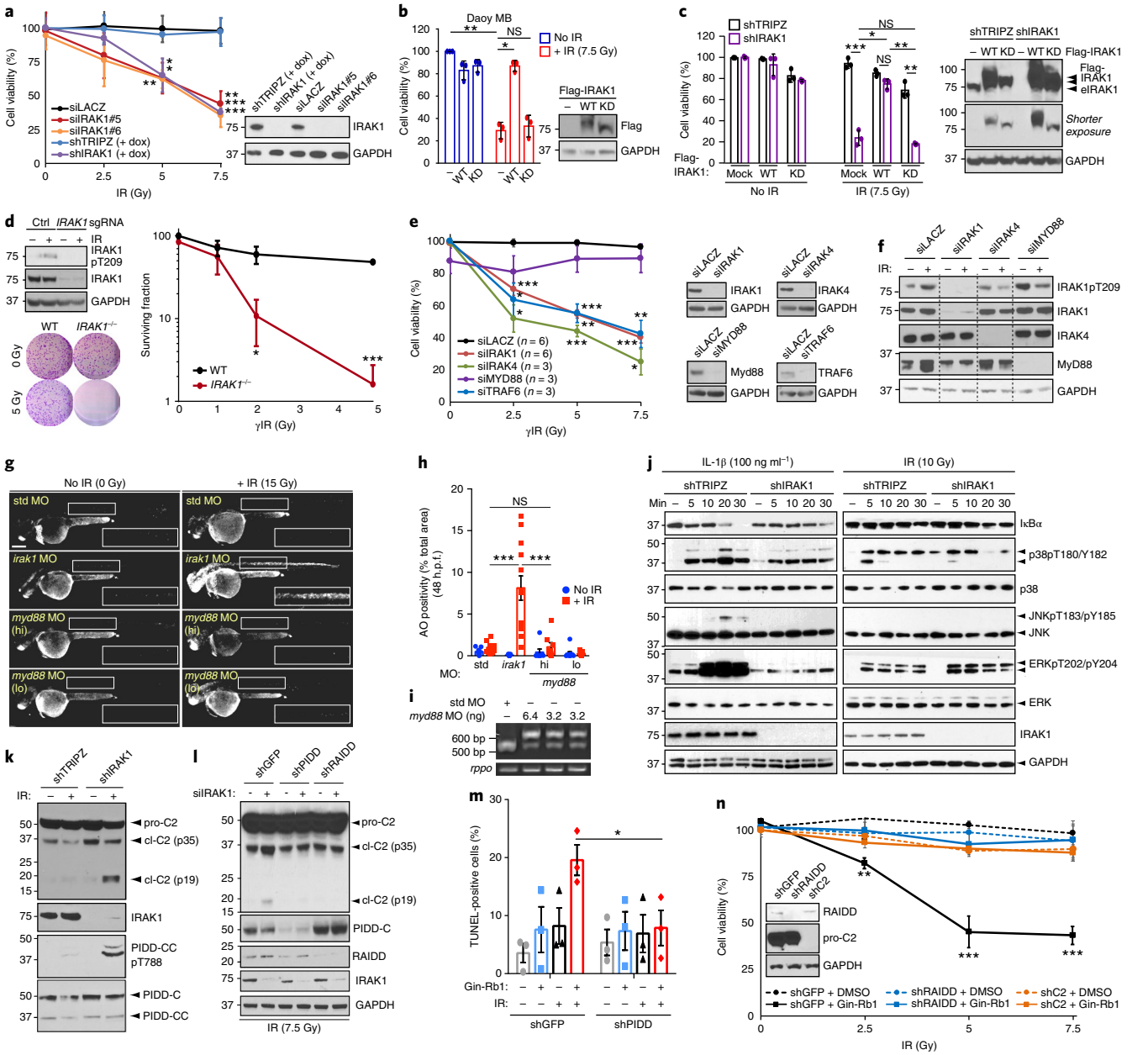

Fig. 4 | IRAK1 acts independently of MyD88 and counters PIDDosome signalling. a–f,j–n, HeLa (**a**,**d**–**f**,**j**–**n**), Daoy MB (**b**) and CAL27 (**c**) cells were transfected with or treated as follows: indicated siRNA (**a**,**e**,**f**); WT or KD Flag-IRAK1 (**b**,**c**); *IRAK1* sgRNA plus Cas9 plasmid (**d**) and/or stably expressing indicated doxycycline (dox)-inducible shRNA (**a**,**c**,**k**) or non-inducible shRNA (**l**–**n**), and/or treated with IRAK1 inhibitor ginsenoside-Rb1 (10 μg ml^{-1}) (**m**,**n**). Cells were then analysed as follows: 5 dpIR (IR doses in Gy) by AlamarBlue cell viability assay (**a**–**c**,**e**,**n**); 14 dpIR by clonogenic assay (**d**); 2 dpIR by TUNEL assay (**m**) and/or by western blotting with the indicated antibodies (**a**–**f**,**j**–**l**) at indicated minutes post-IR or IL-1β treatment (**j**); or 24 hpIR (**a**–**f**,**k**,**l**,**n**). eIRAK1, endogenous IRAK1; pro-C2, procaspase-2; cl-C2 (p35), intermediate cleavage product; cl-C2 (p19), mature cleavage product. Data in **a**–**e** and **m**,**n** are presented as the mean ± s.d., $n = 3$ independent experiments performed in triplicate. In **j**, activation of the following pathways are marked as follows: by a gradual decline in IκB levels (NF-κB); p38 T180/Y182 phosphorylation (p38 MAPK); JNK T183/Y185 phosphorylation (JNK); ERK T202/Y204 phosphorylation (ERK). **g**,**h**, Representative images (as in Fig. 3b for std and *irak1* MOs) and quantification of *p53*$^{MK/MK}$ embryos injected with indicated MOs and treated with or without 15 Gy IR at 18 h.p.f. and analysed in an AO assay at 24 hpIR. Number of quantified spinal chord images (as boxed in **g**) from 4 independent experiments (bars 1–4) or 3 independent experiments (bars 5–8) were as follows: std MO: n of non-irradiated = 9, n of irradiated = 11; *irak1* MO: n of non-irradiated = 11, n of irradiated = 13; *myd88* MO high (hi, 6.4 ng): n of non-irradiated = 7, n of irradiated = 8; *myd88* MO low (lo, 3.2 ng): n of non-irradiated = 9, n of irradiated = 11. **i**, RT-PCR of pooled embryo mRNA extracts shows MO dose-dependent intron retention in *myd88* messages. $^*P < 0.05$, $^{**}P < 0.005$, $^{**}P < 0.0005$ throughout the figure (two-tailed Student's t-test). See Supplementary Table 4 for statistics source data, including precise P values, and Supplementary Fig. 8 for unprocessed immunoblots. Scale bar, 0.2 mm (for all panels).

and T98G cells (Fig. 5d; Supplementary Fig. 5). In stark contrast, ginsenoside-Rb1 and R406 radiosensitized up to 10 and 7 of 11 *TP53* mutant lines, respectively (Daoy MB excluded) (see Fig. 5d and Supplementary Fig. 5 for corresponding cell viability curves, and Supplementary Fig. 4d–f for select colony assays). MCF7 radioresistance could not be overcome throughout the screen regardless

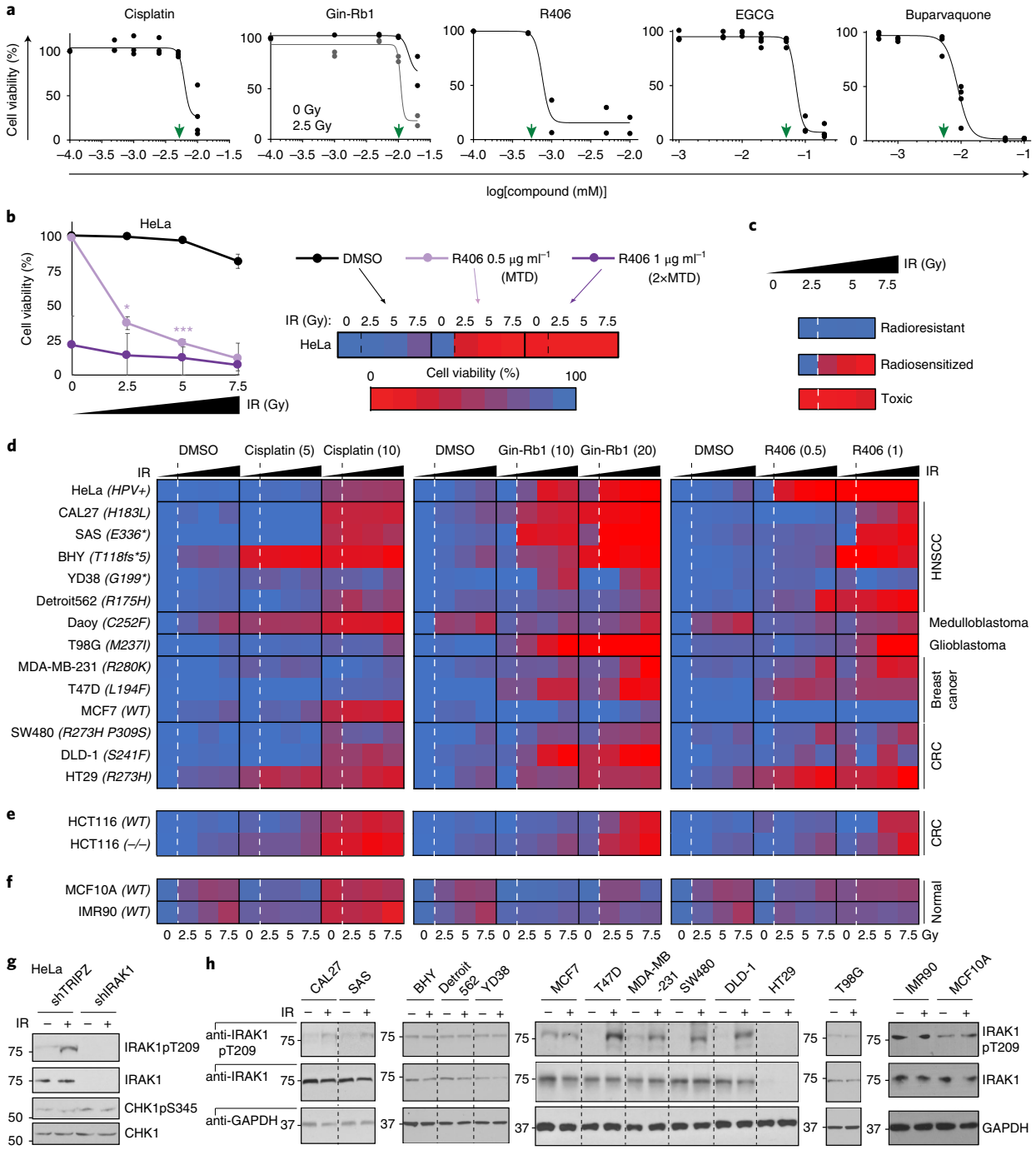

Fig. 5 | IRAK1 inhibitors restore radiosensitivity across *TP53* mutant tumour cell models. a, AlamarBlue-based HeLa cell viability assays establish MTDs (green arrowheads) for cisplatin, the IRAK1 inhibitors ginsenoside-Rb1 (Gin-Rb1) and R406, and the PIN1 inhibitors EGCG and buparvaquone. Gin-Rb1 required 2.5 Gy to achieve MTD at doses below the precipitation point of the drug. $n = 2$ independent experiments in triplicate, data are presented as the means. **b**,**c**, Explanatory schematic for the heatmap shown in **d**, with R406 on IR-treated HeLa cells as the example. **b**, Cells treated with MTD (0.5 μg ml^{-1}) and 2×MTD (1 μg ml^{-1}) with 3 doses of IR represented in a standard dose–response curve (left) and corresponding heatmap representation (right). Cell viability colour code shown from red at 0% to blue at 100%. Note that this example showcases the three main phenotypic classes observed in the screen shown in **d**: radioresistant, radiosensitized and toxic (individually depicted in **c**). Data are presented as the mean of $n = 3$ independent experiments. $^{*}P < 0.05$, $^{***}P < 0.0005$ (two-tailed Student's *t*-test). Source data available in Table 4, sheet S5. **d**–**f**, AlamarBlue-based cell viability heatmaps of radioresistant cancer cell lines. Cell line names indicated to the left with *TP53* genotype in parentheses and tumour of origin to the right (**d**), WT and *TP53*-null HCT116 cells (**e**) and normal human cells (MCF10A, IMR90; **f**) treated with cisplatin or IRAK1 inhibitors, Gin-Rb1 and R406, at indicated doses (MTD and 2×MTD, in μg per ml) and IR (0, 2.5, 5 and 7.5 Gy, as indicated) in $n = 3$ independent experiments performed in triplicate. Corresponding survival curves and *P* values are shown in Supplementary Fig. 5. **g**, Indicated HeLa shRNA lines treated with or without IR (10 Gy) and analysed by western blotting at 24 hpIR. **h**, Cell lines as in **d** treated with or without IR (10 Gy) and analysed by western blotting 24 hpIR. A total of 7 of 9 lines (HeLa, CAL27, SAS, T47D, MDA-MB-231, SW480 and DLD-1, see **d**) reliably radiosensitized by IRAK1 inhibitors engage IRAK1 phosphorylation in response to IR, while both resistant lines (BHY, MCF7) do not. See Supplementary Table 4 for statistics source data, including precise *P* values, and Supplementary Fig. 8 for unprocessed immunoblots.

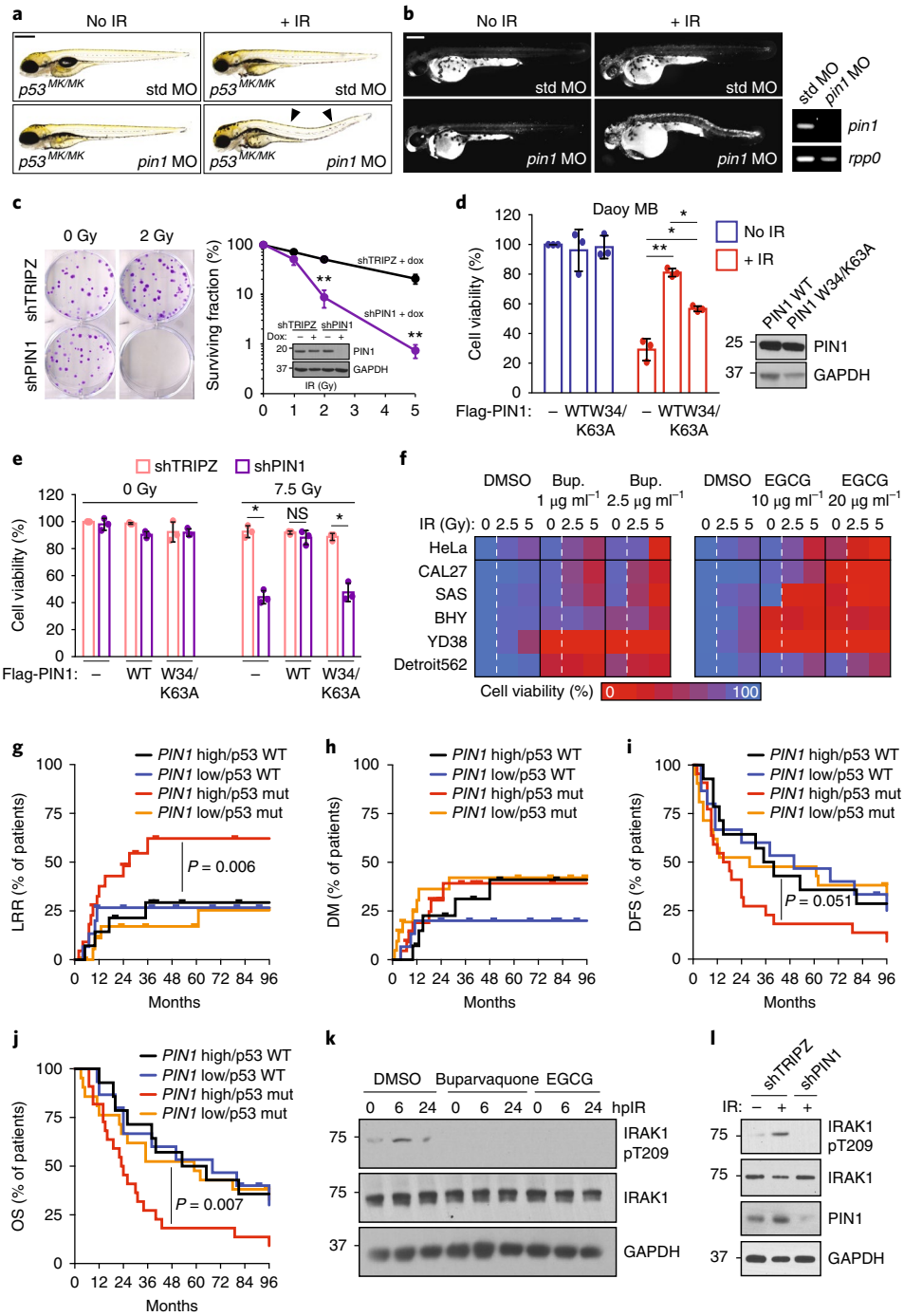

Fig. 6 | PIN1 inhibition overcomes R-RT in zebrafish and human tumour-cell models while its overexpression associates with *TP53* mutant HNSCC recurrence. a,**b**, MO depletion of PIN1 but not std MO restores DTCs (**a**) and AO uptake (**b**) after 15 Gy IR. See Supplementary Fig. 6c,d for quantifications. **b**, Right: RT–PCR of embryonic mRNA extracts detect nonsense mediated decay of *pin1* mRNA. **c**, Clonogenic assay of shTRIPZ and shPIN1 HeLa cells after up to 5 Gy IR. Surviving fractions to the right. Western blot of PIN1 knockdown also shown in the inset. **d**, Daoy MB cells transfected with mock, WT or catalytically inactive (W34/K63A) PIN1 exposed to 0 or 7.5 Gy IR and assayed by AlamarBlue at 5 dpIR. Western blot of Flag-PIN1 levels also shown. **e**, shTRIPZ and shPIN1 CAL27 cells reconstituted with Flag-PIN1 constructs exposed to 0 or 7.5 Gy IR and assayed by AlamarBlue at 5 dpIR. Data in **c**–**e** are the mean ± s.d. of $n = 3$ independent experiments performed in triplicate. $^*P < 0.05$, $^{**}P < 0.005$ (two-tailed Student's *t*-test). **f**, MTD and 2×MTD of buparvaquone (Bup.) and EGCG given to indicated cell lines with 0, 2.5 or 5 Gy IR and analysed by AlamarBlue in $n = 3$ independent experiments in triplicate. Colour coding as in Fig. 5d. Corresponding survival curves including *P* values shown in Supplementary Fig. 6n. **g**–**j**, Kaplan–Meier curves showing LRR (**g**), distant metastases (DM, **h**), disease-free survival (DFS, **i**) and overall survival (OS, **j**) in patients from the MD Anderson Cancer Center HNSCC cohort split at median *PIN1* expression and analysed by two-sided log-rank test. All patients treated with complete surgical resection followed by post-operative RT. Number of patients were as follows: $PIN1^{high}/TP53$ WT, $n = 14$; $PIN1^{low}/TP53$ WT, $n = 15$; $PIN1^{high}/TP53$ mutant (mut), $n = 22$; $PIN1^{low}/TP53$ mutant, $n = 21$. See Supplementary Table 3 for patient characteristics. **k**,**l**, HeLa cells treated with buparvaquone (1 μg ml^{-1}) or EGCG (10 μg ml^{-1}) (**k**) or stably expressing indicated shRNAs (**l**) treated with 0 or 10 Gy IR and analysed by western blot at indicated hpIR. See Supplementary Table 4 for statistics source data, including precise *P* values, and Supplementary Fig. 8 for unprocessed immunoblots.

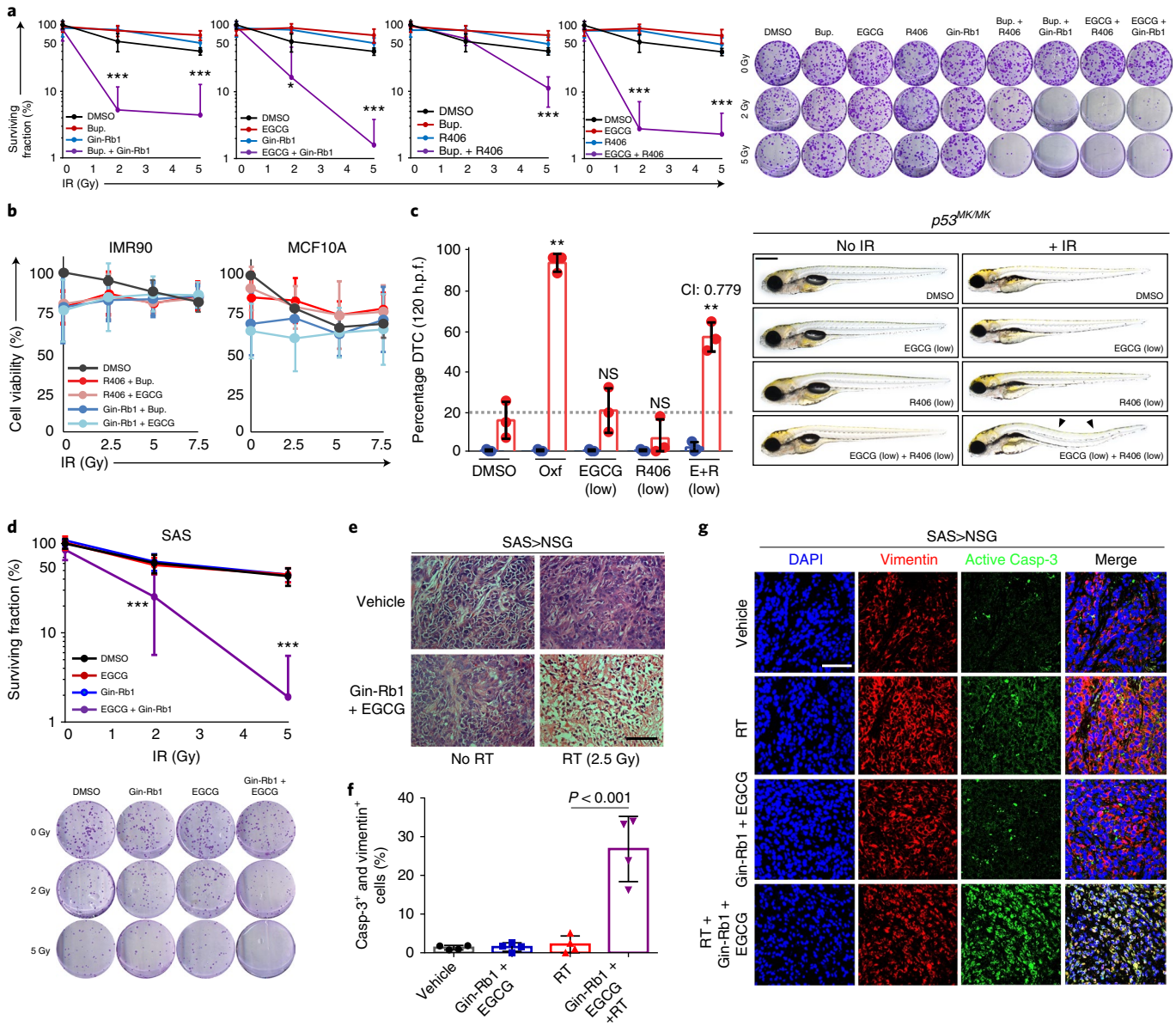

Fig. 7 | Low-dose IRAK1 and PIN1 inhibitors synergistically suppress R-RT in vitro and in vivo. a,**b**, HeLa (**a**) and non-tumorigenic IMR90 and MCF10A cells (**b**) treated with indicated IRAK1 and PIN1 inhibitors at subtherapeutic doses (buparvaquone (0.5 μg ml^{-1}), R406 (0.1 μg ml^{-1}), ginsenoside-Rb1 (5 μg ml^{-1}) and EGCG (5 μg ml^{-1}); see Fig. 5a) and indicated γIR doses (Gy) and analysed by clonogenic assay at 14 dpIR (**a**, with representative images to the right) or AlamarBlue at 5 dpIR (**b**). Data are presented as the mean ± s.d. of $n = 3$ independent experiments (**a**, **b**, left) and $n = 4$ independent experiments (**b**, right) performed in triplicate. **c**, *p53*$^{MK/MK}$ embryos treated with subtherapeutic doses of EGCG (40 μg ml^{-1}) and R406 (20 μg ml^{-1}) and 0 or 15 Gy TBI at 18 h.p.f. analysed for DTCs at 120 h.p.f. Data are presented as the mean ± s.d. of $n = 3$ independent experiments, with representative images shown to the right. *P* value is relative to DMSO-treated irradiated embryos (bar 2). CI, combination index (see Supplementary Fig. 7f). Scale bar, 0.5 mm. **d**, Surviving fractions of SAS cells treated with subtherapeutic doses of ginsenoside-Rb1 (5 μg ml^{-1}) and/or EGCG (5 μg ml^{-1}) at indicated IR exposures (Gy), analysed 14 dpIR. Representative images shown below. Data are presented as the mean ± s.d. of $n = 3$ independent experiments performed in triplicate. **e**–**g**, SAS (2×10^6 cells)-derived tumour xenografts grown in NSG mice with $n = 5$ animals per indicated group analysed by haemotoxylin and eosin staining (**e**) and immunofluorescence confocal microscopy with indicated antibodies (**f**,**g**) 24 days post-implantation. See Methods for detailed implantation, RT, drug delivery and staining protocols. Scale bars, 100 μm (**e**) and 80 μm (**g**). Data in **f** are from the analysis of $n = 4$ independent samples per group with 3 independent images (as in **g**) scored per tumour. Anti-vimentin and anti-active caspase-3 mark human and apoptotic cells, respectively. Unless otherwise indicated, data throughout are expressed as the mean ± s.d., $^*P < 0.05$, $^{**}P < 0.005$, $^{***}P < 0.0005$ (two-tailed Student's *t*-test). See Supplementary Table 4 for statistics source data, including precise *P* values.

of drug, drug dose or IR dose. In the great majority of cases, radiosensitization by the IRAK1 inhibitors occurred in those lines that engaged IRAK1 T209 phosphorylation in response to IR (Fig. 5g,h). Radiosensitization was also obtained at drug doses that were tolerated in the absence of IR (see 0 Gy data points in Fig. 5d and Supplementary Fig. 5) and in irradiated non-tumorigenic fibroblasts (IMR-90) and mammary epithelial cells (MCF10A) (Fig. 5f; Supplementary Fig. 5). Taken together with the zebrafish and HeLa

data, these results identified IRAK1 as a target for inhibition in cancers with mutant *TP53*-driven R-RT.

An additional predicted oxfendazole target, PIN1 isomerase, drives R-RT in zebrafish and tumour-cell models and associates with R-RT in HNSCC. Following our analysis of SEA-predicted oxfendazole targets, we noted that inhibition of one additional candidate target, the peptidyl-prolyl *cis/trans* isomerase PIN1[42], radiosensitized zebrafish $p53^{MK/MK}$ mutants with a similar potency to that of the IRAK1/4 inhibitor (Fig. 2a,b). While in vitro isomerase and thermal shift assays could not immediately confirm PIN1 as an oxfendazole target (Supplementary Fig. 6a,b), genetic or pharmacological inhibition of PIN1 did consistently suppress R-RT in zebrafish (Fig. 6a,b; Supplementary Fig. 6c–g), in HeLa cells (Fig. 6c; Supplementary Fig. 6i,j) and in HNSCC lines (see Fig. 6e,f and Supplementary Fig. 6n for corresponding cell viability curves, and Supplementary Fig. 6j–m for select colony assays). Similar to IRAK1, PIN1 was sufficient to force R-RT when overexpressed in radiosensitive Daoy MB cells, whereas a catalytically inactive (W34A/K63A) variant[43] was less potent (Fig. 6d). In further support of PIN1 as a driver of tumour R-RT, overexpression of *PIN1* was significantly associated with locoregional recurrence (LRR; $P=0.006$) and reduced overall survival ($P=0.007$), but not distant metastases, in patients with *TP53* mutant HNSCC who were treated with postoperative RT at the MD Anderson Cancer Center[11,44] (Fig. 6g–j; Supplementary Table 3). Inspection of TCGA HNSCC cohort—whose analysis is however limited by a lack of LRR data[45]—revealed significant upregulation of *PIN1* in *TP53* mutant tumours that were ultimately treated with RT (Supplementary Fig. 3f–h).

PIN1 inhibition prevents IR-induced IRAK1 activation and synergizes with IRAK1 inhibitors in vitro and in vivo. Interestingly, PIN1 plays an essential and direct role in TLR-induced IRAK1 activation[46]. Similarly, we found that genetic or pharmacological inhibition of PIN1 blocked IR-induced IRAK1 phosphorylation on T209 (Fig. 6k,l). We therefore tested whether IRAK1 and PIN1 inhibitors synergistically suppress R-RT in our various models. We trialled four combinations of IRAK1 + PIN1 inhibitors, involving the IRAK1 inhibitors ginsenoside-Rb1 and R406 (see above), and the PIN1 inhibitors epigallocatechin gallate (EGCG), a competitive inhibitor with micromolar efficacy shown to bind the PIN1 catalytic site[47,48], and buparvaquone, a repurposed antiparasitic that binds and inhibits PIN1 with nanomolar efficacy[49]. Each inhibitor was titrated to a dose that did not decrease HeLa survival as a single agent, even after 2.5 or 5 Gy IR. Under these subtherapeutic conditions, all four combination treatments produced marked synergistic declines in survival specifically after IR (see Fig. 7a and Supplementary Fig. 7a,e and for combination indexes). These findings were recapitulated in the following models: $p53^{MK/MK}$ fish (Fig. 7c; Supplementary Figs. 6h and 7f); *TP53* mutant HNSCC cell lines grown in vitro (Fig. 7d; Supplementary Fig. 7b–d,g) or as tumour xenografts in vivo (Fig. 7e–g; Supplementary Fig. 7h); $TP53^{-/-}$ as well as WT HCT116 cells (Supplementary Fig. 7i); and one of the cell lines from our radioresistant panel that best resisted IRAK1 inhibitors as single agents (SW480 cells; Supplementary Fig. 7b,g). All four IRAK1 + PIN1 inhibitor combinations were otherwise tolerated in IMR90 human fibroblasts, including after up to 7.5 Gy IR (Fig. 7b, left). While MCF10A mammary epithelial cells showed some sensitivity (Fig. 7b, right), such toxicity was not further exacerbated by IR and was marginal compared with the levels of tumour-cell lethality induced by the various drug combinations in the tumorigenic cell lines (for example, compare 5 Gy data points in Fig. 7b to that in Supplementary Fig. 7a,b). Clinical translation will require extending these studies to additional in vivo tumour models and *TP53* alleles, including in immunocompetent mice. Together, our data collectively identify IRAK1 and PIN1 as rational targets in radioresistant cancers, with efficacy stemming from single or low-dose combination treatments.

Discussion

The data presented here show that IRAK1, a core transducer in innate immune signalling conserved from flies to humans[23,24,27], plays an additional conserved role in the cell survival response to IR. This pathway involves the IL-1R/TLR pathway members PIN1, IRAK4 and TRAF6. However, its MyD88-independence, full reliance on IRAK1 kinase activity, partial reliance on TRAF6 and divergent downstream target (the PIDDosome) are supportive of a distinct stress-response pathway that diverged from, or possibly preceded, the pathogen response. The pathway may respond to one or more IR-induced primary or secondary ionization events, including DNA breakage, micronucleation or other occurrences of cytosolic DNA, hydroxyl radicals or other reactive oxygen species. Ruptured lipid bilayers and/or so-called danger-associated molecular patterns (that is, DNA or nuclear proteins released into extracellular space) may also trigger the pathway[50,51]. A key feature of this pathway from a therapeutic viewpoint is its IR-induced essentiality, whereby pathway inhibition is lethal to zebrafish or cancer cells exposed to IR but is otherwise tolerated in the absence of IR. Even germline losses of *Irak1* or *Pin1* are viable in mice[52,53]. Thus, IRAK1 inhibitor treatment (alone or with a PIN1 inhibitor) could lead to improved tumour radiosensitization strategies whereby drug-induced cytotoxicity is restricted to the field of RT with minimal effects in unexposed tissues. Additionally, the radiosensitzing properties of IRAK1 and PIN1 inhibitors in *TP53* mutant tumour cells are not allele-specific and are largely retained in $TP53^{-/-}$ and WT backgrounds. This potentially expands the patient population that might benefit from IRAK1 ± PIN1 inhibitor-based CRT. Finally, recent reports implicate deregulated *IRAK1* and *PIN1* in tumour progression, maintenance and metastasis, via stabilization of mutant p53 itself[54] and other pathways[23,32,34,42]. Our discovery of these enzymes as drivers of cellular R-RT calls for further development of IRAK1 and PIN1 inhibitors for therapeutic use.

Online content

Any methods, additional references, Nature Research reporting summaries, source data, statements of data availability and associated accession codes are available at https://doi.org/10.1038/s41556-018-0260-7.

Received: 6 June 2018; Accepted: 7 December 2018;
Published online: 21 January 2019

References

1. Lawrence, Y. R. et al. NCI-RTOG translational program strategic guidelines for the early-stage development of radiosensitizers. *J. Natl Cancer Inst.* **105**, 11–24 (2013).
2. Sharma, R. A. et al. Clinical development of new drug–radiotherapy combinations. *Nat. Rev. Clin. Oncol.* **13**, 627–642 (2016).
3. Wilson, G. D., Bentzen, S. M. & Harari, P. M. Biologic basis for combining drugs with radiation. *Semin. Radiat. Oncol.* **16**, 2–9 (2006).
4. Golden, E. B., Formenti, S. C. & Schiff, P. B. Taxanes as radiosensitizers. *Anticancer Drugs* **25**, 502–511 (2014).
5. Adelstein, D. J. et al. An intergroup phase III comparison of standard radiation therapy and two schedules of concurrent chemoradiotherapy in patients with unresectable squamous cell head and neck cancer. *J. Clin. Oncol.* **21**, 92–98 (2003).
6. Olivier, M. et al. The IARC TP53 database: new online mutation analysis and recommendations to users. *Hum. Mutat.* **19**, 607–614 (2002).
7. Igney, F. H. & Krammer, P. H. Death and anti-death: tumour resistance to apoptosis. *Nat. Rev. Cancer* **2**, 277–288 (2002).
8. Vogelstein, B., Lane, D. & Levine, A. J. Surfing the p53 network. *Nature* **408**, 307–310 (2000).
9. Vousden, K. H. & Lu, X. Live or let die: the cell's response to p53. *Nat. Rev. Cancer* **2**, 594–604 (2002).
10. Poeta, M. L. et al. TP53 mutations and survival in squamous-cell carcinoma of the head and neck. *N. Engl. J. Med.* **357**, 2552–2561 (2007).

11. Skinner, H. D. et al. TP53 disruptive mutations lead to head and neck cancer treatment failure through inhibition of radiation-induced senescence. *Clin. Cancer Res.* **18**, 290–300 (2012).
12. Nam, T. K. et al. Molecular prognostic factors in rectal cancer treated by preoperative chemoradiotherapy. *Oncol. Lett.* **1**, 23–29 (2010).
13. Sclafani, F.et al. TP53 mutational status and cetuximab benefit in rectal cancer: 5-year results of the EXPERT-C trial. *J. Natl Cancer Inst.* **106**, dju121 (2014).
14. Eikesdal, H. P., Knappskog, S., Aas, T. & Lonning, P. E. TP53 status predicts long-term survival in locally advanced breast cancer after primary chemotherapy. *Acta Oncol.* **53**, 1347–1355 (2014).
15. Li, S., Zhang, W., Chen, B., Jiang, T. & Wang, Z. Prognostic and predictive value of p53 in low MGMT expressing glioblastoma treated with surgery, radiation and adjuvant temozolomide chemotherapy. *Neurol. Res.* **32**, 690–694 (2010).
16. Tabori, U. et al. Universal poor survival in children with medulloblastoma harboring somatic TP53 mutations. *J. Clin. Oncol.* **28**, 1345–1350 (2010).
17. Berghmans, S. et al. tp53 mutant zebrafish develop malignant peripheral nerve sheath tumors. *Proc. Natl Acad. Sci. USA* **102**, 407–412 (2005).
18. Sidi, S. et al. Chk1 suppresses a caspase-2 apoptotic response to DNA damage that bypasses p53, Bcl-2, and caspase-3. *Cell* **133**, 864–877 (2008).
19. McAleer, M. F. et al. Novel use of zebrafish as a vertebrate model to screen radiation protectors and sensitizers. *Int. J. Radiat. Oncol. Biol. Phys.* **61**, 10–13 (2005).
20. Lacey, E. Mode of action of benzimidazoles. *Parasitol. Today* **6**, 112–115 (1990).
21. Prichard, R. K. & Ranjan, S. Anthelmintics. *Vet. Parasitol.* **46**, 113–120 (1993).
22. Keiser, M. J. et al. Relating protein pharmacology by ligand chemistry. *Nat. Biotechnol.* **25**, 197–206 (2007).
23. Jain, A., Kaczanowska, S. & Davila, E. IL-1 receptor-associated kinase signaling and its role in inflammation, cancer progression, and therapy resistance. *Front. Immunol.* **5**, 553 (2014).
24. Janssens, S. & Beyaert, R. Functional diversity and regulation of different interleukin-1 receptor-associated kinase (IRAK) family members. *Mol. Cell* **11**, 293–302 (2003).
25. Powers, J. P. et al. Discovery and initial SAR of inhibitors of interleukin-1 receptor-associated kinase-4. *Bioorg. Med. Chem. Lett.* **16**, 2842–2845 (2006).
26. Wang, Z. et al. Crystal structures of IRAK-4 kinase in complex with inhibitors: a serine/threonine kinase with tyrosine as a gatekeeper. *Structure* **14**, 1835–1844 (2006).
27. O'Neill, L. A., Golenbock, D. & Bowie, A. G. The history of Toll-like receptors—redefining innate immunity. *Nat. Rev. Immunol.* **13**, 453–460 (2013).
28. Rolf, M. G. et al. In vitro pharmacological profiling of R406 identifies molecular targets underlying the clinical effects of fostamatinib. *Pharmacol. Res. Perspect.* **3**, e00175 (2015).
29. Joh, E. H., Lee, I. A., Jung, I. H. & Kim, D. H. Ginsenoside Rb1 and its metabolite compound K inhibit IRAK-1 activation–the key step of inflammation. *Biochem. Pharmacol.* **82**, 278–286 (2011).
30. Yao, J. et al. Interleukin-1 (IL-1)-induced TAK1-dependent versus MEKK3-dependent NFkappaB activation pathways bifurcate at IL-1 receptor-associated kinase modification. *J. Biol. Chem.* **282**, 6075–6089 (2007).
31. Kollewe, C. et al. Sequential autophosphorylation steps in the interleukin-1 receptor-associated kinase-1 regulate its availability as an adapter in interleukin-1 signaling. *J. Biol. Chem.* **279**, 5227–5236 (2004).
32. Wee, Z. N. et al. IRAK1 is a therapeutic target that drives breast cancer metastasis and resistance to paclitaxel. *Nat. Commun.* **6**, 8746 (2015).
33. Muroi, M. & Tanamoto, K. IRAK-1-mediated negative regulation of Toll-like receptor signaling through proteasome-dependent downregulation of TRAF6. *Biochim. Biophys. Acta* **1823**, 255–263 (2012).
34. Rhyasen, G. W. & Starczynowski, D. T. IRAK signalling in cancer. *Br. J. Cancer* **112**, 232–237 (2015).
35. Conze, D. B., Wu, C. J., Thomas, J. A., Landstrom, A. & Ashwell, J. D. Lys63-linked polyubiquitination of IRAK-1 is required for interleukin-1 receptor- and toll-like receptor-mediated NF-kappaB activation. *Mol. Cell. Biol.* **28**, 3538–3547 (2008).
36. Ando, K. et al. PIDD death-domain phosphorylation by ATM controls prodeath versus prosurvival PIDDosome signaling. *Mol. Cell* **47**, 681–693 (2012).
37. Sladky, V., Schuler, F., Fava, L. L. & Villunger, A. The resurrection of the PIDDosome—emerging roles in the DNA-damage response and centrosome surveillance. *J. Cell Sci.* **130**, 3779–3787 (2017).
38. Tinel, A. & Tschopp, J. The PIDDosome, a protein complex implicated in activation of caspase-2 in response to genotoxic stress. *Science* **304**, 843–846 (2004).
39. Tinel, A. et al. Autoproteolysis of PIDD marks the bifurcation between pro-death caspase-2 and pro-survival NF-kappaB pathway. *EMBO J.* **26**, 197–208 (2007).
40. Barretina, J. et al. The Cancer Cell Line Encyclopedia enables predictive modelling of anticancer drug sensitivity. *Nature* **483**, 603–607 (2012).
41. Essmann, F., Engels, I. H., Totzke, G., Schulze-Osthoff, K. & Janicke, R. U. Apoptosis resistance of MCF-7 breast carcinoma cells to ionizing radiation is independent of p53 and cell cycle control but caused by the lack of caspase-3 and a caffeine-inhibitable event. *Cancer Res.* **64**, 7065–7072 (2004).
42. Lu, Z. & Hunter, T. Prolyl isomerase Pin1 in cancer. *Cell Res.* **24**, 1033–1049 (2014).
43. Wei, S. et al. Active Pin1 is a key target of all-trans retinoic acid in acute promyelocytic leukemia and breast cancer. *Nat. Med.* **21**, 457–466 (2015).
44. Skinner, H. D. et al. Proteomic profiling identifies PTK2/FAK as a driver of radioresistance in HPV-negative head and neck cancer. *Clin. Cancer Res.* **22**, 4643–4650 (2016).
45. Cancer Genome Atlas Network Comprehensive genomic characterization of head and neck squamous cell carcinomas. *Nature* **517**, 576–582 (2015).
46. Tun-Kyi, A. et al. Essential role for the prolyl isomerase Pin1 in Toll-like receptor signaling and type I interferon-mediated immunity. *Nat. Immunol.* **12**, 733–741 (2011).
47. Moore, J. D. & Potter, A. Pin1 inhibitors: pitfalls, progress and cellular pharmacology. *Bioorg. Med. Chem. Lett.* **23**, 4283–4291 (2013).
48. Urusova, D. V. et al. Epigallocatechin-gallate suppresses tumorigenesis by directly targeting Pin1. *Cancer Prev. Res. (Phila.)* **4**, 1366–1377 (2011).
49. Marsolier, J. et al. *Theileria* parasites secrete a prolyl isomerase to maintain host leukocyte transformation. *Nature* **520**, 378–382 (2015).
50. Candeias, S. M. & Testard, I. The many interactions between the innate immune system and the response to radiation. *Cancer Lett.* **368**, 173–178 (2015).
51. Reisz, J. A., Bansal, N., Qian, J., Zhao, W. & Furdui, C. M. Effects of ionizing radiation on biological molecules–mechanisms of damage and emerging methods of detection. *Antioxid. Redox. Signal.* **21**, 260–292 (2014).
52. Thomas, J. A. et al. Impaired cytokine signaling in mice lacking the IL-1 receptor-associated kinase. *J. Immunol.* **163**, 978–984 (1999).
53. Liou, Y. C. et al. Role of the prolyl isomerase Pin1 in protecting against age-dependent neurodegeneration. *Nature* **424**, 556–561 (2003).
54. Girardini, J. E. et al. A Pin1/mutant p53 axis promotes aggressiveness in breast cancer. *Cancer Cell* **20**, 79–91 (2011).

Acknowledgements

The authors thank E. Farias, R. Cagan, A. Dar, R. Krauss, J. Ashwell, X. Li, M. Posner, P. Reddy, R. De Vita and R. Sanchez for helpful comments, technical advice and reagents, and C. Franco and D. Dominguez for zebrafish care. This work was supported in part by the following bodies: NIH/NCI (F30CA186448 to P.H.L.; P30 CA008748 to K.S.P.; RO1CA168485 to H.D.S. and J.V.H; and RO1CA178162 to S.S.); the National Cancer Center NCC CCP (postdoctoral fellowship (to Y.L.); and the JJR Foundation, the Pershing Square Sohn Cancer Research Alliance, the New York Community Trust and the Searle Scholars Program (to S.S.).

Author contributions

P.H.L. performed the following experiments: zebrafish drug screen with the assistance of J.M.B and V.B.; all zebrafish experiments with the exception of the TUNEL and caspase-3 assays (V.B.), and the p53atgMO, myd88MO, and hIRAK1 WT, K/R and E3A rescue assays (Y.L); and SEA analyses under the supervision of A.S. and S.S. R.B.S. performed all the cell culture assays with the assistance of P.H.L. and R.T., and analysed the data with P.H.L., Y.L. and S.S. R.G.M. purchased the radioresistant cell lines and assisted with translational analyses with J.A.A.-G. E.d.S., R.M.W., J.A.A.-G. and S.S. conceived the xenograft study, which was performed by E.d.S. and analysed by R.R. A.A. performed TCGA analyses under the supervision of K.S.P. and analysed the data with R.M.W. and S.S. P.M.-U.U. performed docking studies under the supervision of A.S. A.G. generated the IRAK1 KO under the supervision of J.M.S. S.K. and X.Z.Z. performed the in vitro isomerase assays under the supervision of K.P.L. H.D.S. analysed *PIN1* expression levels in the MD Anderson Cancer Center HNSCC cohort with the assistance of J.V.H. S.S. conceived the study, supervised the project and wrote the paper.

Competing interests

The authors declare no competing interests.

Additional information

Supplementary information is available for this paper at https://doi.org/10.1038/s41556-018-0260-7.

Reprints and permissions information is available at www.nature.com/reprints.

Correspondence and requests for materials should be addressed to S.S.

Publisher's note: Springer Nature remains neutral with regard to jurisdictional claims in published maps and institutional affiliations.

Methods

Zebrafish lines and maintenance. Adult zebrafish were maintained on a 14:10 h light:dark cycle at 28 °C in accordance with the regulations and policies of the Mount Sinai Institutional Animal Care and Use Committee. The study is compliant with all relevant ethical regulations regarding zebrafish research. The progeny of $p53^{MK/MK}$ fish were used in most experiments. WT zebrafish were from the AB line. The TILLING-mediated generation of the $p53^{MK/MK}$ line, including allele designation, has been previously described[17,18].

Zebrafish drug screen. Live embryos were dechorionated in pronase (2.0 mg ml^{-1} in egg water) for 7 min and rinsed three times in egg water at 17 h.p.f. At least 15 $p53^{MK/MK}$ embryos were then arrayed into each well of a 24-well plate and treated with drugs from FDA-approved drug library V1 (Enzo Life Sciences) or proprietary kinase inhibitors (Reddy Lab) at a final concentration of 20 µg ml^{-1} in egg water. In the primary screen, three wells were set aside for controls: one negative control, $p53^{MK/MK}$ + DMSO; and two positive controls, $p53^{MK/MK}$ + Gö6956 (1 µM) and $p53^{+/+}$ + DMSO. Plates containing drug-treated embryos were γ-irradiated at 18 h.p.f. using a ^{137}Cs-irradiator (X-ray IR can also be used, but developmental stage and dose differ, presumably due to low-energy electrons). At 6 hpIR, embryos were washed three times and scored at 72 h.p.f. and 120 h.p.f. for curved tails and gross morphological changes. If any well lost embryos to necrosis or manipulation such that fewer than 12 embryos were left before 120 h.p.f., that data point was not included in the analysis and the entire condition was repeated. In the secondary screen, the set-up was similar except two 24-well plates were set-up with identical drug treatments identified in the primary screen, with embryos randomly assigned to each plate. Phenotyping was identical to the primary screen. Again, at least 12 embryos were required to survive until 120 h.p.f. for the data point to be counted, and the secondary screen was performed in three independent experiments. Pictures were obtained of tricaine-anaesthetized embryos mounted on 2–3% methylcellulose and imaged with a Nikon SMZ 1500 fluorescence microscope.

Acridine orange labelling. Live embryos were dechorionated in pronase (2.0 mg ml^{-1} in egg water) for 7 min and rinsed three times in egg water at 17 h.p.f. After being arrayed and incubated with drugs, depending on the experiment, embryos were then γ-irradiated at 18 h.p.f. using a ^{137}Cs-irradiator. At 6 hpIR, embryos were labelled live with acridine orange at 10 mg ml^{-1} in egg water for 20 min, washed three times and analysed using ImageJ as previously described[18].

Whole-mount TUNEL staining and caspase-3 immunohistochemistry. The TUNEL cell death assay was performed according to the manufacturer's instructions (ApopTag Fluorescein In Situ Apoptosis Detection kit) with zebrafish manipulations as previously described[18]. Embryos stained for caspase-3 or γH2AX were fixed in 4% paraformaldehyde overnight at 4 °C and subsequently dehydrated in methanol at −20 °C for at least 2 h. Embryos were then rehydrated three times for 5 min in PBST (1× PBS, 0.1% Tween-20), and permeabilized by treatment with PDT (PBST, 1% DMSO) supplemented with 0.3% Triton-X for 20 min. Embryos were treated with blocking solution (PDT supplemented with 10% heat-inactivated fetal bovine serum (FBS)) for 30 min before the addition of primary antibody (1:500 anti-activated-caspase-3 (StressGen AAs-103), 1:200 anti-γH2AX (Millipore, 05–636)). Embryos were incubated in primary antibody overnight at 4 °C, rinsed three times for 20 min in PDT and then re-blocked for 30 min in blocking solution before the addition of AlexaFluor-conjugated secondary antibody (1:250). Immunohistochemistry for TUNEL- and caspase-3-labelled embryos were imaged with a Nikon SMZ 1500 fluorescence microscope. Immunohistochemistry for γH2AX was imaged with a Leica SP5 DM confocal microscope.

SEA analysis. Chemical compound SMILES formulas were queried with the online SEA search tool (http://sea.bkslab.org/search/), searching against ChEMBL v.16 Binding 10 µM. Results for the found benzimidazoles were copied into Microsoft Excel, sorted for duplicates and colour graded according to *E*-values.

TCGA analysis. TCGA datasets for two cancer types (HNSCC and breast cancer) were obtained from the Broad Institute's Firehose pipeline. Gene expression data were quantile normalized via RSEM and $\log_2$ transformed before analyses for IRAK1 and PIN1. *TP53* mutation status and radiation therapy treatment are summarized for each cancer type. Wilcoxon rank-sum test was performed to test the association between gene (*IRAK1*, *PIN1*) expression and *TP53* mutation status and receipt of radiation therapy. We further analysed *IRAK1* and *PIN1* expression in *TP53* mutant and WT groups across patients who received RT versus those who did not. Survival comparisons were made via a log rank test. Each gene was stratified with respect to its median expression across *TP53* status to determine any prognostic association. All analyses were done in R software v.3.4.2 including the 'survival' package. Note that, receipt of radiation is a time varying covariate that can confound survival association through the time it was administered. Date of receipt of radiation is needed to perform this analysis, which is not included in the TCGA dataset[55].

Chemicals and inhibitors. Oxfendazole, fluocinolone, exemestane, cefepime, pranlukast, amiloride, alfacalcidol and albendazole were obtained from VWR. Amoxapine, ricobendazole and mercazole were obtained from Sigma-Aldrich. Salmeterol, indomethacin, canthaxanthin, bifonzole, rapamycin, mebendazole, fenbendazole and flubendazole were obtained from Santa Cruz Biotechnologies. Misoprostol was obtained from Thermo Fisher, while rebastinib and regorafenib were obtained from Selleck Chem. Gö6976 was obtained from Calbiochem, while lapatinib, SB203580 and SB202190 were gifts from J.A.A.-G. Dabrafenib, sorafenib and vemurafenib were gifts from A. Dar. Recombinant human IL-1β was from Peprotech (200-01B). Doxycycline hyclate was purchased from Sigma (D9891-1G). The following inhibitors were used in this study: IRAK1/4 inhibitor (Sigma, I5409); R406 (Selleck Chemicals, S2194); ginsenoside-Rb1 (Abcam, ab142646, and J&K Scientific, 112127); buparvaquone (Santa Cruz Biotechnology, sc-210970); and EGCG (Sigma, E4268 and E4143). The IRAK1/4 inhibitor was originally discovered in a high-throughput small-molecule screen for IRAK inhibitors, with IC_{50} values of 300 nM and 200 nM for IRAK1 and IRAK4, respectively. For 27 other kinases tested during discovery, IC_{50} values were >10,000 nM[25]. Ginsenoside-Rb1 was originally isolated from ginseng extract and identified as a saponin among other components extracted from ginseng. It inhibits IRAK1 in an in vitro kinase assay with an IC_{50} of ~10 µM[29], with other reported activities against PI3K, AKT, ER-β and enhancement of the NRF2–HO-1 pathway, among others. R406 was originally found to be a SYK inhibitor with an inhibition constant (K_i) of 30 nM[56], although DiscoverX assays (described below) showed it to also inhibit FLT3, as well as IRAK1 and IRAK4. EGCG was identified as a polyphenolic compound found in green tea, with its earliest effects proposed to be a protectant against the carcinogenic effects of teleocidin and okadaic acid[57]. It was later found to directly bind and inhibit PIN1 with a K_i of 20 µmol per litre[48]. Buparvaquone was derived from a series of anti-*Theileria parva* (a cattle parasite) compounds, with its primary proposed mechanism as inhibiting the parasite cytochrome *b*. It was recently found to also inhibit *Theileria annulate* PIN1 in vitro (no reported IC_{50} or $K_d$values)[49].

In vitro kinase-binding assays (KINOMEScan). KINOMEScan assays (DiscoverX) were performed as follows: kinase-tagged T7 phage strains were prepared in an *Escherichia coli* host derived from the BL21 strain. *E. coli* were grown to log-phase and infected with T7 phage and incubated with shaking at 32 °C until lysis. The lysates were centrifuged and filtered to remove cell debris. The remaining kinases were produced in HEK-293 cells and subsequently tagged with DNA for quantitative PCR (qPCR) detection. Streptavidin-coated magnetic beads were treated with biotinylated small-molecule ligands for 30 min at room temperature to generate affinity resins for kinase assays. The liganded beads were blocked with excess biotin and washed with blocking buffer (SeaBlock (Pierce), 1% BSA, 0.05% Tween 20, 1 mM dithiothreitol (DTT)) to remove unbound ligand and to reduce nonspecific binding. Binding reactions were assembled by combining kinases, liganded affinity beads and test compounds in 1× binding buffer (20% SeaBlock, 0.17× PBS, 0.05% Tween 20, 6 mM DTT). Test compounds were prepared as 111× stocks in 100% DMSO. K_d values were determined using an 11-point threefold compound dilution series with three DMSO control points. All compounds for K_d measurements were distributed by acoustic transfer (non-contact dispensing) in 100% DMSO. The compounds were then diluted directly into the assays such that the final concentration of DMSO was 0.9%. All reactions were performed in polypropylene 384-well plates. Each reaction contained a final volume of 0.02 ml. The assay plates were incubated at room temperature with shaking for 1 h and the affinity beads were washed with wash buffer (1× PBS, 0.05% Tween 20). The beads were then re-suspended in elution buffer (1× PBS, 0.05% Tween 20, 2 µM non-biotinylated affinity ligand) and incubated at room temperature with shaking for 30 min. The kinase concentration in the eluates was measured by qPCR.

In vitro kinase assays. In vitro kinase assays were performed by Reaction Biology Corporation. Briefly, substrate (myelin basic protein (MBP), 20 µM final) was freshly prepared in reaction buffer (20 mM HEPES, pH 7.5, 10 mM MgCl2, 1 mM EGTA, 0.02% Brij35, 0.02 mg ml^{-1} BSA, 0.1 mM Na_3VO_4, 2 mM DTT, 1% DMSO). Human IRAK1 kinase (4 nM) was added to the substrate solution, followed by oxfendazole by acoustic technology (Echo550; nanolitre range). Samples were incubated for 20 min at room temperature before addition of ^{33}P-ATP (10 µM final concentration, with specific activity of 10 µCi µl^{-1}), then incubated for 2 h at room temperature. Radioactivity was detected using the filter-binding method. Kinase activity data are expressed as the percentage remaining kinase activity in test samples compared to vehicle (DMSO) reactions. Oxfendazole was tested in 10-dose IC_{50} mode in triplicate with threefold serial dilution starting at 200 µM, control compound staurosporine was tested in 10-dose IC_{50} mode with fourfold serial dilution starting at 20 µM. IC_{50} values and curve fits were obtained using Prism (GraphPad Software).

Molecular docking. Protein sequences of the IRAK1 and IRAK4 catalytic domains were aligned with T-Coffee's structure-based alignment mode, Expresso[58]. The IRAK4 X-ray structure (2nru)[26] was used as the template for homology modelling of IRAK1. The homology modelling program MODELLER v.9.15[59] was used to generate ten IRAK1 models with an average ZDOPE[60] score of −0.64 ± 0.06,

suggesting that at least 70% of the atoms are within 3.5 Å of the native IRAK1 structure. Molecular docking to the IRAK1 models was performed with Glide, using the Standard Precision mode and a hydrogen-bond constraint at the hinge region. The docking results from the models were combined to generate the consensus docking result[61]. Oxfendazole and analogues are predicted to dock to the ATP-binding site and to interact with the hinge region with the benzimidazolyl carbamate moiety, while the phenylsulfoxide moiety resides in a pocket adjacent to the DFG motif. The method for zebrafish IRAK1 homology modelling was the same as for human IRAK1. Default settings were used for induced-fit docking of oxfendazole. Specifically, the scaling of van der Waals radii for the receptor atom was changed to 0.75 for atoms with a charge larger than $\pm 0.15\,e$[62].

Microinjections into zebrafish embryos. Human IRAK1 WT, KD and K134R/K180R were subcloned into the pCS2+ plasmid using restriction enzymes EcoRI and XhoI. The IRAK1 E3A-pCS2+ construct was generated using a Q5 Site-Directed Mutagenesis kit (NEB, E0552S) to produce the E3A variant[63]. All plasmids were linearized by Sac2 single enzyme treatment at 37 °C for 4 h. Digests were stopped by adding 1/20 volume 0.5 M EDTA, 1/10 volume of 3 M sodium acetate and 2 volumes ethanol. Samples were mixed and chilled at −20 °C for 15 min, washed and resuspended in TE buffer. Sense-capped mRNAs were synthesized for injection using a mMESSAGE mMACHINE SP6 kit (Ambion, AM1340) following the manufacturer's instructions. mRNA concentrations were determined using a Nanodrop spectrophotometer and by RNA gel electrophoresis. The following mRNAs were co-injected with *irak1* morpholinos during the 1–2 cell stage: 20 pg WT *IRAK1* mRNA, 25–30 pg IRAK1 KD, 25–30 pg K134R/K180R or 25–30 pg E3A mutant mRNAs. The *zp53*-ATG morpholino[64] and zp53-specific[64] antibody (Genetex, GTX128135) were provided by J. Chu. Protein extractions from embryos were performed as previously described[3] and analysed by western blotting as described below. Morpholino antisense oligonucleotides were obtained from Gene Tools. Sequences are as follows:Standard control (std): 5′-CCTCTTACCTCAGTTACAATTTATA-3′

pin1-e1i1: 5′-ACTCTCTCTGCTCACTCTGGATGAG-3′
irak1-i5e6: 5′-AATCCTGCAACACAACAGCCACATT-3′
irak4-e4i4: 5′-GTGAACAGGTAAAGCCTCACAGGAT-3′
zp53-ATG: 5′-GCGCCATTGCTTTGCAAGAATTG-3′
myd88: 5′-TCTTGACGGACTGGGAAACTC G-3′.

Morpholinos were resuspended in sterile water to a stock concentration of 2 mM and delivered into one-cell stage zebrafish embryos by microinjection at various final concentrations with 0.1% phenol red (Sigma).

Sequencing primers for confirming knockdown were as follows:
rpp0-F: TAGCCGATCCGCAGACACAC
rpp0-R: CTGAACATCTCGCCCTTCTC
pin1-e1-F: AGAACATCACACGCAGCAAAG
pin1-e3-R: GTGCAAATGAGGCGTCTTCAA
irak1-e1-F: GGGTTATGGACTCGCTTTCA
irak1-e11-R: CATGCGAGGTCTCTTCTTC
Myd88F: TCTTGACGGACTGGGAAACTCG
Myd88R: GATTTGTAGACGACAGGGATTAGCC.

PCR with reverse transcription (RT–PCR) and protein extraction from zebrafish embryos. Embryonic RNA was isolated from 24–48 h.p.f. embryos (>15 embryos per sample) using a standard TRIzol method (250 µl TRIzol (Invitrogen), 50 µl $CHCl_3$, 175 µl isopropanol). One microgram of purified RNA was used to generate complimentary DNA using an Invitrogen SuperScript First Strand III RT–PCR kit, with oligo-dT primers. Two micrograms of the cDNA product was loaded on a 1% agarose gel. Pooled embryo protein lysates were collected as previously described[18].

Cell culture and cell lines. HeLa, HCT116, CAL27, SAS, BHY, HN and Detroit562 cell lines were cultured in DMEM medium (Gibco) supplemented with 10% FBS and 1% penicillin–streptomycin. YD38 cells were cultured in RPMI medium, also supplemented with 10% FBS and 1% penicillin–streptomycin. Experiments requiring combined drug treatment and irradiation were performed as follows: cells were seeded in 10-cm plates and grown to 30–50% confluence. One hour before IR, cells were treated with indicated drugs. Collection of lysates for western blotting after IR typically occurred at 24 hpIR, while collection of cells for fixation and TUNEL staining occurred at 48 hpIR. CAL27, Detroit562, Daoy MB and T98G cells were obtained from American Type Culture Collection. SAS cells were purchased from Health Science Research Resources Bank, BHY from Deutsche Sammlung von Mikroorganismen und Zellkulturen, and YD38 from Korean Cell Line Bank. MDA-MB-231, T47D and MCF7 cells were provided by D. Germain. HeLa stable shPIDD, shRAIDD and shCASP2 cells have been previously described[36]. IMR90 and MCF10A cells were provided by J.A.A.-G. See Supplementary Table 3 for more details on cell line-specific culture media and protocols.

siRNA transfection, shRNA transduction, DNA transfection and constructs. Short interfering RNA (siRNA) transfections were performed using X-tremeGENE siRNA transfection reagent (Roche) and, unless otherwise stated, with 20 nM siRNA according to the manufacturer's instructions. Cells were exposed to IR alone or with Gö6976 or oxfendazole at 48 h post-transfection. Lentiviral short hairpin RNA (shRNA) transduction was performed in HeLa cells as previously described[36] with shTRIPZ, shPIN1 and shIRAK1. shPIDD, shRAIDD and shCASP2 HeLa cells and hairpin sequences have been previously described[36]. DNA transfections were performed as previously described[65]. Human IRAK1 WT and KD[30] were gifts from X. Li. IRAK1 human IRAK1 K134R/K180R in pDEST-515 vector[35] was from J. Ashwell. IRAK1 E3A, derived from WT IRAK1 template, was generated using a Q5 Site-Directed Mutagenesis Kit (NEB, E0552S) to produce the E544A/E587A/E706A mutations[63]. pBybe-PIN1-WT and pBybe-PIN1-W34K63A have been previously described[66]. siRNAs were also provided by Qiagen, and target sequences were as follows:

siIRAK1#5: CCGGGCAATTCAGTTTCTACA
siIRAK1#6: TCCCATCGCCATGCAGATCTA
siIRAK4#6: ATCCTATTAGTCATATATTTA
siMYD88#5: AACTGGAACAGACAAACTATC
siTRAF6#7: AGGGTACAATACGCCTTACAA
siPIN1#5: GACCGCCAGATTCTCCCTTAA
siPIN1#6: CAGTATTTATTGTTCCCACAA.

shRNA clones were purchased from Qiagen and mature antisense sequences were as follows:

shIRAK1: ATTACTCAAGGACAACCTG (V3THS_305359)
shPIN1.1: TGAAGTAGTACACTCGGCC
shPIN1.2: TGGCTGAGCTGCAGTCGCT.

CRISPR–Cas9 gene editing. Plasmid lentiCRISPR v2 was digested with BbsI (New England Biolabs, R0580) according to the manufacturer's recommendations. Briefly, 1 µg of plasmid was digested for 1 h at 55 °C, then digested plasmid was gel purified using a QIAquick Gel Extraction kit and eluted in water. Single guide RNA oligonucleotides for cloning were annealed by mixing them in equal 10 µM concentrations with the addition of 1×T4 DNA ligase buffer, then the mixture was incubated at 37 °C for 30 min, then at 95 °C for 5 min and then ramped down to 25 °C at 5 °C min^{-1}. Hybridized oligonucleotides were diluted 1:200 with H_2O. BbsI digested lentiCRISPR v2 plasmid (50 ng) was ligated with 1 µM final concentration oligo duplex using T4 Ligase (NEB, M0202) according to the manufacturer's recommendations and incubated overnight at 4 °C. XL-1 blue competent *E. coli* were transformed with 1 µl of ligation reaction according to the manufacturer's protocol (Agilent Technologies, catalogue no. 200249). Single clones were sequence verified using Sanger sequencing. Lentivirus particles containing sgRNA constructs of IRAK1 were generated by transfecting Phoenix packaging cells with lentiCRISPR v2 containing *IRAK1* sgRNAs and a combination of the lentiviral helper plasmids pCMV-dR8.91 and pMD.G at a ratio of 2:1:1, respectively; jetPEI (Polyplus, 101-10N) was used as the transfection agent. After 24 h, medium containing viral particles was collected and concentrated using Lenti-X Concentrator according to the manufacturer's protocol (Clontech, 631231). Briefly, 1 volume of Lenti-X Concentrator was mixed with 3 volumes of 0.45-µm filtered viral particle-containing media. The solution was then incubated overnight at 4 °C. The samples were centrifuged at 1,500×*g* for 45 min at 4 °C, supernatant aspirated and the pellet resuspended in HeLa and CAL27 cell growth media. For infection, 2×10^5 HeLa and CAL27 cells were plated into 6-well plates. The next day, 5 µM polybrene (Millipore, tr-1003-g) and 200 µl of concentrated viral particles were added per well. The medium was replaced the next day with medium containing 1 µg ml^{-1} puromycin for selection.

The IRAK1 sgRNA oligonucleotides (5′ > 3′) were as follows:
sgRNA1:
(1) CACCGACACGGTGTATGCTGTGAAG
(2) AAACCTTCACAGCATACACCGTGTC
sgRNA2:
(1) CACCGAGGAGTACATCAAGACGGGA
(2) AAACTCCCGTCTTGATGTACTCCTC
sgRNA3:
(1) CACCGATTTATCCCACAGAAAGACC
(2) AAACGGTCTTTCTGTGGGATAAATC
sgRNA4:
(1) CACCGGATCAACCGCAACGCCCCGTG
(2) AAACCACGGGCGTTGCGGTTGATCC.

AlamarBlue cell survival assay. Cells were seeded into 96-well plates at densities ranging from 400 to 1,500 cells per well (see Supplementary Table 3 for seeding densities). Eight hours after seeding, if experiments were performed on cells in which shRNA was not previously transfected, drugs were added to the medium, incubated for 1 h, then irradiated. If shRNA lines were used, cells were treated with 1 µg ml^{-1} doxycycline for 24 h before irradiation. At 3–4 days post IR, cells were incubated with AlamarBlue (ThermoFisher) at a final concentration of 10%. Absorbance was measured at a wavelength of 570 nm with a 600 nm reference wavelength. Relative fluorescence was calculated using cell-free wells as a control reference, and percentage survival was calculated by comparing with DMSO-treated, non-IR controls.

Clonogenic assay. Single-cell suspensions were seeded into 6-well plates (50–200 cells per well). Drugs were added to the medium after 8 h and irradiated in a ^{137}Cs-irradiator. After being cultured for 14 days, plates were rinsed with PBS, incubated with fixing solution (75% methanol, 25% acetic acid) and stained with 0.5% crystal violet (Sigma-Aldrich) in methanol for 30 min at room temperature. Colonies consisting of at least 50 cells were scored. Clonogenic assays performed on shRNA-transfected lines required media to be refreshed with 1 μg ml^{-1} doxycycline every 48 h.

TUNEL assay (cell lines). TUNEL assays in HeLa cells were performed using an APO-BRDU kit (BD Biosciences) as described previously[18].

Western blotting and antibodies. Whole-cell lysates were prepared in RIPA buffer or 1% NP-40 Buffer (Boston BioProducts). Lysate (25–200 μg) was added to NuPAGE LDS Sample Buffer (4×, Invitrogen) and 5% 2-mercaptoethanol (Sigma), and samples were incubated at 70 °C for 10 min. Samples were run on a Tris-acetate gel in MES running buffer (Invitrogen). After electrophoresis, samples were transferred for 2 h (90 V, 150–200 mA) to a nitrocellulose membrane (Thermo Scientific) using a submerged transfer apparatus (Bio-Rad). Membranes were then blocked with 5% BSA in Tris-buffered saline with 0.1% Tween (TBST) and probed overnight at 4 °C with primary antibodies. Membranes were then washed in TBST and probed with anti-rabbit, -rat or -mouse (Cell Signaling Technology) horseradish peroxidase-linked antibodies at a 1:2,000–4,000 dilution for 1 h. After washing, the membranes were placed in SuperSignal West Pico Chemiluminescent Substrate or SuperSignal West Dura Extended Duration Substrate (Pierce Biotechnology). The band of interest was then identified by photographic film. The following antibodies were used: anti-γH2AX (Ser139) (Cell Signaling Technology, 9718); anti-CHK1 (clone G-4, Santa Cruz Biotechnologies, sc-8408); anti-CHK1pSer345 (clone 13303, Cell Signaling Technology, 2348); anti-PIDD (anti-LRDD, clone Anto1, Novus Biologicals, NBP1-97595); anti-RAIDD (clone 4B12, MBL); anti-PIDDpT788 (custom-generated, see ref. [31]); anti-caspase-2 (clone 11B4, EMD Millipore, MAB3507); anti-IRAK1 (Cell Signaling Technology, 4504); anti-IRAK1pT209 (Assay Biotech, A1074); anti-IRAK1pS376 (Genetex, 55332); anti-IRAK4 (Cell Signaling Technology, 4363); anti-ERKpT202/Y204 (Cell Signaling Technology, 4370); anti-ERK1/2 (Cell Signaling Technology, 4696); anti-p38pT180/Y182 (Cell Signaling Technology, 4511); anti-p38 (BD Biosciences, 610168); anti-JNKpT183/Y185 (Santa Cruz Biotechnologies, sc-6254); anti-IκBα (Cell Signaling Technology, 4814); anti-TRAF6 (Santa Cruz Biotechnologies, sc-8409); anti-MyD88 (Cell Signaling Technology, 4283); anti-PIN1 (Abcam, ab53350); anti-actin (Abcam, ab8227); anti-CHK2 (clone 7, Millipore); anti-p-CHK2 (T68) (Cell Signaling Technology, 2661); anti-GAPDH (Cell Signaling Technology, 2118); anti-Flag (DYKDDDDK Tag antibody, Cell Signaling Technology, 2368).

Immunofluorescence and confocal microscopy (cell culture). HeLa cells (1×10^5) were seeded on coverslips in 6-well plates, fixed in 1% paraformaldehyde, permeabilized in 0.2% Triton X-100, blocked in 1% BSA–PBS, stained with IRAK1 antibody (1:100) and secondary antibody (1:200, anti-rabbit, AlexaFluor 488, Invitrogen), mounted in Vectashield with 4,6-diamidino-2-phenylindole (DAPI) and sealed with nail polish, as described previously[65]. Images were obtained under a ×63 NA 1.40 oil objective with an inverted confocal microscope (405 nm, 488 nm; SP5, Leica) and acquired using LAS software.

Prolyl isomerase assay. The prolyl isomerase (PPIase) activity on glutathione *S*-transferase (GST)-PIN1, GST-FKBP12 or GST-cyclophilin in response to compounds were determined using the chymotrypsin-coupled PPIase activity assay with the substrate Suc-Ala-pSer-Pro-Phe-pNA, Suc-Ala-Glu-Pro-Phe-pNA or Suc-Ala-Ala-Pro-Phe-pNA (50 mM) in buffer containing 35 mM HEPES (pH 7.8), 0.2 mM DTT and 0.1 mg ml^{-1} BSA at 10 °C, as described previously[67]. K_i values obtained from the PPIase assay were derived from the Cheng–Prusoff equation ($K_i = IC_{50}/(1 + S/K_m)$), where K_m is the Michaelis constant for the used substrate, S is the initial concentration of the substrate in the assay, and the IC_{50} value of the inhibitor, as previously described[67]. ATRA (R2625), cyclosporin A (300224) and FK-506 (F4679) were all purchased from Sigma.

Thermal shift assay. Two micrograms of recombinant PIN1 (VWR) was combined with EGCG, oxfendazole, buparvaquone and nocodazole at 100 μM and Protein Thermal Shift Buffer (Applied Biosciences). Mixtures were incubated at room temperature for 20 min, combined with Thermal Shift dye and subjected to differential scanning fluorimetry[68]. Melt reactions from 20 to 90 °C in 1 °C increments were performed using a StepOne Plus instrument (Applied Biosciences). Fluorescence readings were acquired with excitation and emission wavelengths of 580 ± 10 nm and 621 ± 14 nm, respectively. StepOne Plus Protein Thermal Shift Software (Applied Biosciences) was used to determine the melting temperature (T_m) from each fluorescence profile, and the T_m of a first derivative of the fluorescence data at each temperature was used to calculate ΔT_m values.

Quantification of synergistic drug interactions. The synergy experiments were performed in both cell culture AlamarBlue survival and zebrafish DTC assays as described above. Subtherapeutic doses were chosen based on dose–response curves with the highest possible dose that produced <10% decrease in cell viability or <20% DTCs after IR in cell culture and zebrafish assays, respectively. This established our MTD. We then chose a dose at a fivefold decrease from the MTD and used both doses for synergy experiments, with one IRAK1 inhibitor and one PIN1 inhibitor. The analysis of synergy was done using the isobologram and combination-index methods, derived from the Chou–Talalay median-effect principle using CompuSyn software[69].

Clinical samples. Pretreatment HNSCC tumours were examined. All patients were treated with complete surgical resection followed by post-operative RT at the MD Anderson Cancer Center. Tumour characteristics are shown in Supplementary Table 3. All studies involving human samples were approved by the MD Anderson Cancer Center Institutional Review Board in accordance with appropriate ethical regulations regarding research involving patient samples. Patient samples were collected as part of clinical protocols with appropriate consent. A total of 72 p16-negative tumours were analysed, for which both p53 status and *IRAK1* and *PIN1* expression were available. Ion torrent sequencing was performed as described previously to examine *TP53* status[44]. mRNA expression was examined using llumina HumanWG-6 V3 BeadChip human whole-genome expression arrays as described previously[44]. For the outcomes analysis, patients were first placed into two groups (36 in each group) according to the expression level of *IRAK1*, *IRAK4*, *TRAF6* or *PIN1* (high versus low) and then further classified by *TP53* status (WT versus mutant). Multivariate analysis of clinical (tumour stage, nodal stage and tumour site) and mRNA-based (*IRAK1*, *IRAK4*, *TRAF6* and *PIN1*) variables potentially affecting LRR was performed using forward stepwise Cox regression for the entire population as well as for only the patients harbouring *TP53* mutations. Kaplan–Meier curves expressing LRR, time to distant metastasis, disease-free survival and overall survival were generated, and log rank statistics were used to determine significance between groups. R software, SPSS statistical software (v.20) and GraphPad Prism were used. For the multivariate analysis for the entire patient population, no clinical characteristic or gene examined was associated with LRR following RT. However, when LRR was examined in only those patients whose tumours harboured a *TP53* mutation, nodal stage trended towards ($P = 0.057$) and *PIN1* expression was significantly ($P = 0.018$) associated with LRR. Indeed, 64% of patients with a mutation in *TP53* and high levels of *PIN1* had a LRR at 5 years compared with ~25% for patients in all other groups (Fig. 6g, $P = 0.006$).

Xenograft studies. NSG mice (Jackson Laboratories) were used for in vivo studies and were cared for in accordance with guidelines approved by the Memorial Sloan Kettering Cancer Center Institutional Animal Care and Use Committee and Research Animal Resource Center. The study was compliant with all relevant ethical regulations regarding mouse research. Female mice (6–8 weeks old) were injected subcutaneously with 2 million SAS cells together with Matrigel[70]. Once tumours reached an average volume of 100 mm^3 (that is, 6 days post-implantation), mice were randomized into one of the four following treatment groups: (1) Control (saline); (2) localized radiation; (3) ginsenoside-Rb1 + EGCG; (4) radiation + ginsenoside-Rb1 + EGCG. The dosing schedule was as follows: ginsenoside-Rb1 (20 mg per kg) intraperitoneally daily, five times for 3 weeks, EGCG (50 mg per kg) intraperitoneally daily, three times for 3 weeks, localized radiation (2.5 Gy) once on day 1. For the drug + RT combination group, RT was delivered 30 min after dosing the mice with ginsenoside-Rb1 + EGCG. Mice were observed daily throughout the treatment period for signs of morbidity or mortality. Tumours were measured twice weekly using calipers, and the volume was calculated using the following formula: length × width^2 × 0.52. Body weight was also assessed twice weekly. After 3 weeks of treatment, tumour samples were collected for immunoblotting and immunohistochemistry analyses.

Staining of xenograft sections. For immunofluorescence staining, paraffin-embedded sections were deparaffinized, followed by rehydration and antigen retrieval as described below. Paraffin-embedded tissue sections were kept at 60 °C in the oven for 15 min, followed by slide hydration in xylene and a graded alcohol series. For antigen retrieval, heat-induced epitope retrieval was performed using a vegetable steamer by incubating slides in 10 mM citrate buffer for 40 min at 60 °C, followed by a wash in H_20 and PBS. Post washes, cell membranes were permeabilized in 0.1% Triton X-100 in PBS for 5 min at room temperature. For primary antibody staining, sections were blocked with 50 mM NH_4Cl for 15 min at room temperature, followed by blocking with 3% normal goat serum and 3% BSA in PBS for 60 min at room temperature. Binding of the primary antibodies against cleaved caspase-3 (Asp175) rabbit antibody (Cell Signaling Technology, 9661) and vimentin rat antibody (R&D systems, MAB2105) was carried out at 4 °C overnight, followed by PBS (2 × 5 min) washes. Before secondary antibody staining, sections were incubated with 3% normal goat serum and 3% BSA in PBS for 30 min at room temperature. Detection by secondary antibodies, AlexaFluor 488 goat anti-rabbit (Invitrogen, A11008) and AlexaFluor 568 goat anti-rat (Invitrogen, A11077), was carried out at room temperature for 1 h in the dark. Slides were mounted in Vectashield with DAPI (Vector Laboratories, CB-2000), following PBS (3 × 5 min) washes. The degree of immunofluorescence staining was evaluated using a Leica TCS SP5 II confocal laser microscope with DAPI, green fluorescent protein and red fluorescent protein filters. Two sections of each treated tumour and three fields

of each tumour section were imaged at ×60 magnification. For haematoxylin and eosin stainings, images were acquired using a Leica brightfield microscope at a magnification of ×40.

Image analysis using Fiji software. Images were analysed using the open-source processing software Fiji (ImageJ). Vimentin-positive cells were scored for positive cleaved caspase-3 staining. For scoring caspase-3-positive cells, images of samples incubated with secondary antibody, but no primary antibody, were used as background. The brightness and contrast of images was adjusted relative to primary antibody control stainings to identify caspase-3-positive cells in all treated conditions. For this analysis, 3 fields of each tumour section and a total of 12 images, comprising 4 tumour samples for each treated condition, were analysed. Total cell numbers per image were counted and the percentages of caspase-3-positive vimentin cells were calculated. Graphs were plotted using Excel, and *P* values were calculated using Student's *t*-test.

Statistics and reproducibility. With the exception of TCGA and MD Anderson Cancer Center patient cohort studies (see TCGA analysis and Clinical samples sections above), paired two-tailed Students *t*-tests were used to determine *P* values ($\alpha = 0.05$). The log rank test was used to determine *P* values for survival curves. Data in bar graphs are presented as the mean ± s.d. or s.e.m., as indicated in legends, and statistical significance is expressed as follows: $^{*}P < 0.05$, $^{**}P < 0.005$, $^{***}P < 0.0005$, NS, not significant. Embryos from WT or $p53^{MK/MK}$ zebrafish group matings were randomly allocated into experimental groups for irradiation, injections and/or drug treatments. Most experiments were carried out at least twice, and the findings of all key experiments were reliably reproduced. All replicates and precise *P* values are documented in Supplementary Table 4, which states the number of independent samples, embryos and independent experiments.

Reporting Summary. Further information on research design is available in the Nature Research Reporting Summary linked to this article.

Code availability

All codes used are referenced in the Methods sections above.

Data availability

The whole-genome expression array data that support the findings of this study have been deposited in the Gene Expression Omnibus (GEO) under accession code GSE67614. The human HNSCC and breast cancer data were derived from TCGA Research Network: http://cancergenome.nih.gov/. The dataset derived from this resource that supports the findings of this study is available in Supplementary Table 4 (see sheet S3). Source data for Figs. 1e, 2b,d, 3c,e,f, 4a–e,g,h,m,n, 5b,d, 6c–j, 7a–d,f,g and Supplementary Figs. 1b, 2a,b, 3, 4a–f,k,l, 5, 6c–n and 7c,d are provided as Supplementary Table 4. The full image dataset that supports the findings in Fig. 3e,f has been deposited in Figshare at https://doi.org/10.6084/m9.figshare.7427942.

All other data supporting the findings of this study are available from the corresponding author upon reasonable request.

References

55. Anderson, J. R., Cain, K. C. & Gelber, R. D. Analysis of survival by tumor response. *J. Clin. Oncol.* **1**, 710–719 (1983).
56. Braselmann, S. et al. R406, an orally available spleen tyrosine kinase inhibitor blocks Fc receptor signaling and reduces immune complex-mediated inflammation. *J. Pharmacol. Exp. Ther.* **319**, 998–1008 (2006).
57. Fujiki, H. et al. Anticarcinogenic effects of (−)-epigallocatechin gallate. *Prev. Med.* **21**, 503–509 (1992).
58. Notredame, C., Higgins, D. G. & Heringa, J. T-Coffee: a novel method for fast and accurate multiple sequence alignment. *J. Mol. Biol.* **302**, 205–217 (2000).
59. Sali, A. & Blundell, T. L. Comparative protein modelling by satisfaction of spatial restraints. *J. Mol. Biol.* **234**, 779–815 (1993).
60. Eramian, D., Eswar, N., Shen, M. Y. & Sali, A. How well can the accuracy of comparative protein structure models be predicted? *Protein Sci.* **17**, 1881–1893 (2008).
61. Ung, P. M. & Schlessinger, A. DFGmodel: predicting protein kinase structures in inactive states for structure-based discovery of type-II inhibitors. *ACS Chem. Biol.* **10**, 269–278 (2015).
62. Sherman, W., Day, T., Jacobson, M. P., Friesner, R. A. & Farid, R. Novel procedure for modeling ligand/receptor induced fit effects. *J. Med. Chem.* **49**, 534–553 (2006).
63. Ye, H. et al. Distinct molecular mechanism for initiating TRAF6 signalling. *Nature* **418**, 443–447 (2002).
64. Langheinrich, U., Hennen, E., Stott, G. & Vacun, G. Zebrafish as a model organism for the identification and characterization of drugs and genes affecting p53 signaling. *Curr. Biol.* **12**, 2023–2028 (2002).
65. Thompson, R. et al. An inhibitor of PIDDosome formation. *Mol. Cell* **58**, 767–779 (2015).
66. Wei, S. et al. Active Pin1 is a key target of all-trans retinoic acid in acute promyelocytic leukemia and breast cancer. *Nat. Med.* **21**, 457–466 (2015).
67. Yaffe, M. B. et al. Sequence-specific and phosphorylation-dependent proline isomerization: a potential mitotic regulatory mechanism. *Science* **278**, 1957–1960 (1997).
68. Niesen, F. H., Berglund, H. & Vedadi, M. The use of differential scanning fluorimetry to detect ligand interactions that promote protein stability. *Nat. Protoc.* **2**, 2212–2221 (2007).
69. Chou, T. C. Theoretical basis, experimental design, and computerized simulation of synergism and antagonism in drug combination studies. *Pharmacol. Rev.* **58**, 621–681 (2006).
70. Kawata, M. et al. Additive effect of radiosensitization by 2-deoxy-D-glucose delays DNA repair kinetics and suppresses cell proliferation in oral squamous cell carcinoma. *J. Oral Pathol. Med.* **46**, 979–985 (2017).

nature research

Corresponding author(s): Samuel Sidi

Reporting Summary

Nature Research wishes to improve the reproducibility of the work that we publish. This form provides structure for consistency and transparency in reporting. For further information on Nature Research policies, see Authors & Referees and the Editorial Policy Checklist.

Statistical parameters

When statistical analyses are reported, confirm that the following items are present in the relevant location (e.g. figure legend, table legend, main text, or Methods section).

n/a	Confirmed	
☐	☒	The exact sample size (*n*) for each experimental group/condition, given as a discrete number and unit of measurement
☐	☒	An indication of whether measurements were taken from distinct samples or whether the same sample was measured repeatedly
☐	☒	The statistical test(s) used AND whether they are one- or two-sided *Only common tests should be described solely by name; describe more complex techniques in the Methods section.*
☒	☐	A description of all covariates tested
☐	☒	A description of any assumptions or corrections, such as tests of normality and adjustment for multiple comparisons
☐	☒	A full description of the statistics including central tendency (e.g. means) or other basic estimates (e.g. regression coefficient) AND variation (e.g. standard deviation) or associated estimates of uncertainty (e.g. confidence intervals)
☐	☒	For null hypothesis testing, the test statistic (e.g. *F*, *t*, *r*) with confidence intervals, effect sizes, degrees of freedom and *P* value noted *Give P values as exact values whenever suitable.*
☒	☐	For Bayesian analysis, information on the choice of priors and Markov chain Monte Carlo settings
☒	☐	For hierarchical and complex designs, identification of the appropriate level for tests and full reporting of outcomes
☐	☒	Estimates of effect sizes (e.g. Cohen's *d*, Pearson's *r*), indicating how they were calculated
☐	☒	Clearly defined error bars *State explicitly what error bars represent (e.g. SD, SE, CI)*

Our web collection on statistics for biologists may be useful.

Software and code

Policy information about availability of computer code

Data collection	No custom code was used to collect data in this study.
Data analysis	All data were analyzed with Microsoft Excel 2016, GraphPad Prism 6, R v3.4.2, MODELLER v9.15, Glide, ImageJ, Fiji and CompuSyn. No custom code was used in our analysis.

For manuscripts utilizing custom algorithms or software that are central to the research but not yet described in published literature, software must be made available to editors/reviewers upon request. We strongly encourage code deposition in a community repository (e.g. GitHub). See the Nature Research guidelines for submitting code & software for further information.

Data

Policy information about availability of data

All manuscripts must include a data availability statement. This statement should provide the following information, where applicable:

- Accession codes, unique identifiers, or web links for publicly available datasets
- A list of figures that have associated raw data
- A description of any restrictions on data availability

The data generated from the primary and secondary screen performed in this study are available from the corresponding author upon reasonable request. All

materials used were commercially available except for 511 unique kinase inhibitors belonging to the OncoNova library, provided by the E. Premkumar Reddy Lab. Sources for all other materials are described in the supplemental materials.

Field-specific reporting

Please select the best fit for your research. If you are not sure, read the appropriate sections before making your selection.

☒ Life sciences ☐ Behavioural & social sciences ☐ Ecological, evolutionary & environmental sciences

For a reference copy of the document with all sections, see nature.com/authors/policies/ReportingSummary-flat.pdf

Life sciences study design

All studies must disclose on these points even when the disclosure is negative.

Sample size	The sample size for the zebrafish drug screen and mechanistic zebrafish experiments was determined with a power analysis based on preliminary experiments. Irradiated p53M214K/M214K embryos treated with DMSO served as the negative control group with a mean penetrance of curved tails of 5% with a standard deviation of 2.8%. Our positive control used irradiated embryos treated with Go6976, which produced curved tails with a mean penetrance of 86% and a standard deviation of 7.6%. This produced a calculated effect size D of 10.6, which was too high for standard power tables. However, in our preliminary experiments, we observed that our negative control embryos never exceeded 20% penetrance, and positive control group never fell below 75% penetrance, so these were used as the difference in mean, with a maximum standard deviation from those preliminary experiments of 28%, establishing a D of 1.6. For two-tailed t-tests with a significance level of 5% and a power of 90%, the number per group required a sample size of n=lO. To account for attrition of embryos due to washing, pronase, or developmental loss as well as to account for pipetting discrepancies, our protocol established that at least 12 embryos be used for condition.
Data exclusions	Exclusion criteria for each zebrafish experiment were as follows: any embryos that were damaged or destroyed during manipulation by washing, pronase treatment, or live imaging were excluded from analysis. Our overall attrition rate due to these manipulations was less than 3% of all embryos used. If any experimental condition (i.e. individual well of zebrafish) yielded exclusion of embryos due to attrition such that the well contained <8 embryos for analysis, the entire condition was excluded due to lack of statistical significance. This condition was then repeated in a new independent experiment. If any 24- or 48-well plate yielded an average attrition rate greater than 3% for all wells in the plate, the experiment was considered compromised and the entire experiment was repeated. Each experiment also contained both negative and positive controls. Negative controls were either nonirradiated AB or p53M214K/M214K for any plate not receiving radiation. For irradiated plates, negative controls were p53M214K/M214K treated with DMSO, and positive controls were p53M214K/M214K embryos treated with Go6976 or oxfendazole in later experiments. Plates were excluded if negative controls yielded phenotypes of >25% AO positivity at 48 hpf or curved tails at 120 hpf OR if positive controls yielded phenotypes of <75% AO positivity or curved tails. For AlamarBlue cell viability experiments, each plate of selected radioresistant cells treated with drugs and subjected to IR contained negative control wells of each cell line treated with DMSO. If IR alone caused a decreased in cell survival relative to non-irradiated controls, with the exception of IR-dose finding experiments or Daoy (described in "Replication" below), the experiment was considered invalid and was repeated.
Replication	All attempts at replication were successful. The primary screen of 640 FDA-approved drugs in zebrafish was not replicated due to its nature as an initial screen. However, if any condition met exclusion criteria, the individual condition was repeated. The secondary screen and all other zebrafish experiments were successfully replicated. The medulloblastoma cell line Daoy were selected based on literature suggesting it was radioresistant, which we could not replicate in AlamarBlue cell viabilities studies. Our data for Daoy were included regardless.
Randomization	For all zebrafish experiments, each independent experiment utilized embryos l collected on different days from randomly selected mating pairs according to parental genotype (e .g. AB wild-type or p53M214K/M214K). Fertilized embryos were then pooled before randomly allocating into experimental conditions (e.g. IR vs no-lR and drug treatments) .
Blinding	The zebrafish drug screen described in Fig. 1b and Supplemental Figs. 2-3 was blinded during data acquisition. The identity of the 640 FDA-approved drugs were blinded to experimenters during both primary and secondary screens. After the top hits were selected based on potency and selectivity, the drugs were unblinded for further study and target discovery.

Reporting for specific materials, systems and methods

Materials & experimental systems

n/a	Involved in the study
☒	☐ Unique biological materials
☐	☒ Antibodies
☐	☒ Eukaryotic cell lines
☒	☐ Palaeontology
☐	☒ Animals and other organisms
☐	☒ Human research participants

Methods

n/a	Involved in the study
☒	☐ ChIP-seq
☒	☐ Flow cytometry
☒	☐ MRI-based neuroimaging

Antibodies

Antibodies used

anti-γH2AX (Ser139) (Cell Signaling Technology #9718);
anti-Chk1 (clone G-4, sc-8408);
anti-Chk1pSer345 (clone 13303, Cell Signaling Technology #2348);
anti-PIDD (anti-LRDD, clone Anto1, Novus Biologicals NBP1-97595);
anti-RAIDD (clone 4B12, MBL);
anti-PIDDpT788 (custom-generated, ref.31);
anti-caspase-2 (clone 11B4, EMD Millipore MAB3507);
anti-IRAK1 (Cell Signaling Technology #4504);
anti-IRAK1pT209 (Assay Biotech, #A1074);
anti-IRAK4 (Cell Signaling Technology #4363);
anti-ERKpT202/Y204 (Cell Signaling Technology #4370);
anti-ERK1/2 (Cell Signaling Technology #4696);
anti-p38pT180/Y182 (Cell Signaling Technology #4511);
anti-p38 (BD Biosciences #610168);
anti-JNKpT183/Y185 (Santa Cruz sc-6254);
anti-IkBa (Cell Signaling Technology #4814);
anti-TRAF6 (Santa Cruz sc-8409);
anti-MyD88 (Cell Signaling #4283);
anti-PIN1 (Abcam ab53350);
anti-actin (Abcam ab8227);
anti-Chk2 (clone 7, Millipore);
anti-p-Chk2 (T68) (#2661, Cell Signaling);
anti-GAPDH (Cell Signaling #2118);
anti-FLAG (DYKDDDDK Tag antibody, Cell Signaling Technology #2368)
Anti-Cleaved Caspase-3 (Asp175) rabbit antibody, Cell Signaling, catalog no.#9661
Anti-activated-Casp-3 Rabbit pAb, StressGen AAs-103
Anti-Vimentin rat antibody, R&D systems, catalog no. MAB2105
Anti-zp53, Genetex, GTX128135

Validation

Antibodies were validated by western blots of control vs. KO or knockdown cells, and/or by functional assays repeating previously reported experiments making use of the antibodies. Additional supporting documentation, references, and validation statements are available at the manufacturer's website.

Eukaryotic cell lines

Policy information about cell lines

Cell line source(s)

HeLa: A. Thomas Look Lab, Dana-Farber
CAL27: ATCC
SAS: HSRRB
BHY: DSMZ
YD38: KCLB
Detroit562: ATCC
MDA-MB-231: Dr. Doris Germain Lab, ISMMS
MCF7: Dr. Doris Germain Lab, ISMMS
T47D: Dr. Doris Germain Lab, ISMMS
SW480: ATCC
DLD-1: ATCC
HT-29: ATCC
Daoy: ATCC
T98G: ATCC
IMR90: Dr. Julio Aguirre-Ghiso Lab, ISMMS
MCF10: Dr. Julio Aguirre-Ghiso Lab, ISMMS
HCT116 p53 WT: A. Thomas Look Lab, Dana-Farber
HCT116 p53 null: A. Thomas Look Lab, Dana-Farber

Authentication

The cells lines were not authenticated.

Mycoplasma contamination	All the cell lines were tested for mycoplasma contamination using Lonza MycoAlert Assay (Cat# LT07-418) using the company's protocol. The cell lines that were mycoplasma-positive were treated with 1 ul of 25mg/ml solution of Plasmocin per 1 ml of medium in the plate. Media was changed every 3 days and plasmocin was added . This process was repeated for 14 days. After the completion of the treatment, the cells were again tested for mycoplasma contamination following the protocol.
Commonly misidentified lines (See ICLAC register)	Of the cell lines used in this study, only MCF7 cells were listed in ICLAC. Our rationale for their use relates to its utility as a commonly used radio-resistant breast cancer cell lines. We chose MBA-MB-231 and T47D as breast cancer cell lines demonstrated to be TP53 mutant as well as radio-resistant. MCF7 cells were also identified as radio-resistant but TP53 wild-type.

Animals and other organisms

Policy information about studies involving animals; ARRIVE guidelines recommended for reporting animal research

Laboratory animals	Details regarding animals used in this study can be found in Methods under "Zebrafish maintenance" and "Xenograft studies". MSG mice (Jackson Laboratories) were used for in vivo xenograft studies and were cared for in accordance with the guidelines approved by the MSKCC IUCAC. Zebrafish were cared for in accordance with the ISMMS IACUC.
Wild animals	This study did not involve wild animals.
Field-collected samples	This study did not involve field-collected samples.

Human research participants

Policy information about studies involving human research participants

Population characteristics	Details regarding patient characteristics in this study, including T stage, N stage, tumor site (oral cavity, oropharynx, hypopharynx or larynx) and TP53 genotype (WT vs. mutant) can be found in Methods under "Clinical Samples", Supplementary Table 3 (Patient Characteristics) and Supplementary Table 4 (sheets 6g-j). All patients were treated with a complete surgical resection followed by post-opertaive RT at MDACC.
Recruitment	All studies involving human samples were approved by the MD Anderson Cancer Center Institutional Review Board in accordance with appropriate ethical regulations regarding research involving patient samples. Patient samples were collected as part of clinical protocols with appropriate consent.